

ABSTRACT

Title of Document: **DEGRADATION ANALYSIS AND HEALTH MONITORING OF LITHIUM ION BATTERIES**

Nicholas Dane Williard, Master of Science, 2011

Directed By: Prof Michael Pecht, Dr. Michael Osterman,
Department of Mechanical Engineering

Degradation and health monitoring of lithium-ion batteries is explored through life-cycle testing and failure analysis. Test samples comprised of four different battery types from two different manufacturers underwent aging and charge/discharge cycling using a variety of load profiles including constant current discharge, pulsed discharge, and varying depths of discharge. Data from in situ monitoring of several parameters including current, voltage, temperature and internal resistance, was analyzed in order to find the best features that could be used to track and characterize battery performance degradation. Degraded samples were disassembled according to a newly developed disassembly methodology that considered the effects of the environment on post-disassembly failure analysis results. Several different failure analysis methods were used in order to gain an understanding of how degradation mechanisms propagate from a materials stand point. Battery electrodes were investigated to observe changes in their chemical and mechanical structures.

**DEGRADATION ANALYSIS AND HEALTH MONITORING OF LITHIUM ION
BATTERIES**

By

Nicholas Dane Williard

Thesis submitted to the Faculty of the Graduate School of the
University of Maryland, College Park, in partial fulfillment
of the requirements for the degree of
Master of Science
Fall 2011

Advisory Committee:
Professor Michael Pecht, Chair
Dr. Michael Osterman
Professor Patrick McCluskey

© Copyright by
Nicholas Williard
2011

Acknowledgements

I would like to thank the Center for Advanced Life Cycle Engineering (CALCE) at the University of Maryland and the more than 100 companies and organizations that support its research annually.

Table of Contents

Table of Contents	iii
1. Introduction	1
General Materials	2
Operation.....	4
Battery Capacity.....	5
Failure Mechanisms	12
1.1 Internal Factors	12
1.2 External factors	18
2. Failure analysis of Lithium Ion batteries	21
Review of Failure Analysis.....	24
<i>Non-Destructive Failure Analysis</i>	24
<i>Destructive Failure Analysis</i>	31
Safety	38
Choosing a Disassembly Environment	43
Disassembly Method.....	48
Post-Disassembly Processing	52
3. Performance Testing	55
Test specimen	55
A Batteries.....	56
CS2 and CX2 Batteries	58
Test Types	61
Cycle Life (Constant Current Discharge)	62
High Rate Discharge Test	63
Pulsed Discharge Tests.....	63
Continuous Charging.....	63
Shallow Charging.....	64
Shelf Life.....	64
Random Cut-off Voltage Test.....	65
4. Results and Discussion	66
Test Results	66
<i>Cycle Life (Constant Current Discharge)</i>	66

<i>High Rate Discharge Test</i>	73
<i>Pulsed Discharge Test</i>	75
<i>Continuous Charging</i>	77
<i>Shallow charging</i>	78
<i>Self Discharge</i>	81
<i>Random Cut-off Voltage Test</i>	83
Failure Analysis Results.....	88
<i>Impedance Spectroscopy Measurements</i>	88
<i>Tape Pull Test</i>	92
<i>Atomic Force Microscopy</i>	94
<i>Scanning Electron Microscope</i>	95
5. Conclusions	97
6. References	99

1. Introduction

Over the past two decades there has been a rise in the portable electronic device industry which, in turn, has fueled the demand for high performance and reliable power sources. To support consumer needs, these electronic applications require rechargeable or secondary batteries that can offer long cycle and storage life, high volumetric and gravimetric energy densities, and high power capabilities [1]. At present, lithium ion batteries exclusively fill this role for portable electronics and are also a major candidate in applications such as plug-in hybrid and electric vehicles, unmanned aerial vehicles, backups on uninterrupted power supplies, and storage of excess energy created through renewable energy technologies such as wind turbines and solar cells.

For practical implementation into next generation technologies, batteries must not only demonstrate favorable performance and reliability characteristics, they must also be accurately monitored in situ to facilitate maintenance and operational based decisions. Battery monitoring typically refers to the evaluation of state of charge (SOC) or the amount remaining charge in a battery before a recharge is required, and state of health (SOH) or the amount of irreversible degradation that has occurred over a battery's life as compared to an unused battery. Most methods of determining these factors require measurements such as current, voltage, internal DC resistance, or electrochemical impedance spectroscopy (EIS). These measurements are then used as inputs into physical or empirically derived models to estimate and predict capacity fade, power fade, discharge voltage, or residual charge. From this information, battery state estimation can be derived.

By establishing a fundamental understanding of battery degradation mechanisms, this text aims to address two critical issues. The first is how physical degradation in lithium-ion cells influences measureable parameters. This information is used to improve battery monitoring techniques by better capturing the behavior of dynamic battery systems though real-time

monitoring. The second issue addresses the effects of degradation at the material level which can ultimately be used to improve material characteristics. By identifying specific physical degradation mechanisms, active steps can be taken to reduce the influence of these mechanisms on susceptible degradation sites. To achieve this, failure analysis is performed and previous methods of failure analysis are reviewed. Specifically the issue of battery disassembly and its effects (from both environmental exposure, and the act of physical disassembly) are critically analyzed.

General Materials

Lithium-based batteries have taken several strides in development since the first commercial lithium-ion (Li-ion) batteries were put on the market by Sony Corporation in 1990 [2]. Most of the advancements in this technology have been made with respect to the chemistry of the battery's active material. Early batteries utilized lithium metal as an anode but encountered several safety issues stemming from undesirable side reactions between lithium metal and the liquid electrolyte which promoted dendrite growth and lead to internal short circuits [1]. Presently, most commercial lithium-based batteries operate on the principal of lithium intercalation and de-intercalation from a carbon graphite anode [3]. So far, graphite has proven to be the best compromise between theoretical capacity and long cycle life. Other materials such as silicon are capable of a higher capacity, but large volume changes upon lithium insertion (up to 300%) results in mechanical damage hindering electrode conductivity and severely reducing cycle life.

Common commercial cathodes use a lithium metal oxide as their active material. In most cases this material is LiCoO_2 due to its long cycle life and storage properties. In these cathodes lithium is in its less reactive ion state (rather than metallic) which allows cells to remain stable during cycling. Other cathode transition metals include nickel in LiNiO_2 which has a higher specific capacity and lower cost but suffers from a shorter cycle life and thermal instability [4].

Also manganese in a LiMn_2O_4 spinel structure has been used as a cathode material. This material has a low cost and is less toxic than LiCoO_2 however it has a lower capacity and suffers further capacity losses due to material phase changes during cycling [5]. Lithium metal phosphates have also been considered as cathode materials. The most common of these uses iron as the transition material to form LiFePO_4 . This material has been studied for its low cost, nontoxic raw materials, stability at high temperatures, and relatively flat discharge voltage curve [6].

Cathodes are usually processed by grinding the active material into a powder form. It is important to control the particle size of this powder as this is an important factor in determining how much surface area will be exposed to the electrolyte for lithium insertion and desorption. Smaller particle sizes are usually associated with higher power applications (due to more surface area available for lithium reaction); however decreasing particle size too much could lead to reliability problems (this will be further discussed in the degradation section). This powder is then mixed with a conductive agent (often graphite) and a polymer binder in order to hold the composite mixture together. Polymer binders are often composed of polyacrylonitrile based latex, styrene-butadiene rubber, poly(butyl acrylate) based latex, or a combination of multiple materials in order to achieve high adhesion strength as well as low surface resistance [7].

The cathode and anode are deposited on current collectors, electrically isolated by a polymer separator, and then would together to form the cell. An electrolyte is added to facilitate ion transport and the entire cell is sealed within a metal or soft foil case with a tab connecting the current collectors to the external leads of the case. Lithium-ion battery manufacturers typically assemble batteries in dry rooms to reduce moisture within the cells. Some manufacturers have introduced glove boxes into their assembly lines for added process control during this step [8]. In solid state batteries, electrolytes are either ceramics or polymers with the most common material being lithium phosphorous oxynitride (LiPON). These types of batteries pose no risk of electrolyte leakage and can be scaled down to very small sizes. Typical lithium-ion batteries have an electrolyte containing a lithium salt, usually Lithium Hexafluorophosphate (LiPF_6) dissolved

in an organic solvent or mixture of organic solvents such as ethylenecarbonate (EC) or diethylcarbonate (DEC). These electrolytes are used for their high conductivity but have sometimes been associated with safety hazards due to their flammability [9]. The separator is a porous polymer material that sits between both electrodes to provide electrical isolation. However the separator must be permeable for the electrolyte in order to provide good ion transport between the anode and the cathode. Separators are generally composed of polyolefins such as polyethylene (PE) or polypropylene. The current collectors are metal foils that provide a conductive pathway from the battery electrodes out to the external circuit. The current collectors also act as a substrate for the active material of the electrodes to be deposited. In most commercial lithium ion batteries, copper is used as the anode current collector while aluminum is used as the cathode current collector. At the very end of the current collector, a thin metal tab is micro-welded to the current collector to provide an electrical connection between the current collector and the external lead of the battery's case.

Operation

During charging, a current is supplied to the cathode, which should have a high standard redox potential. The cathode transition metal is oxidized while positively charged lithium ions are removed from interstitial sites in the cathode and diffuse through the electrolyte and the separator to the anode where they are intercalated into layers of graphite to form Li_xC_6 . Simultaneously, the electrons leaving the oxidized cathode flow though the external circuit in the opposite direction of the current to reduce the anode. At the end of charging, the external circuit is left open, closing the conductive pathway for electrons to flow back to the cathode. Thus energy is stored within the cell. Upon discharge the external circuit is closed and electrons move from the anode while the cathode transition metal is reduced. Lithium ions are deintercalated from the anode and move though the electrolyte back to the cathode (Figure 1). The reversibility of these redox reactions is what defines the cycle life of a particular cell.

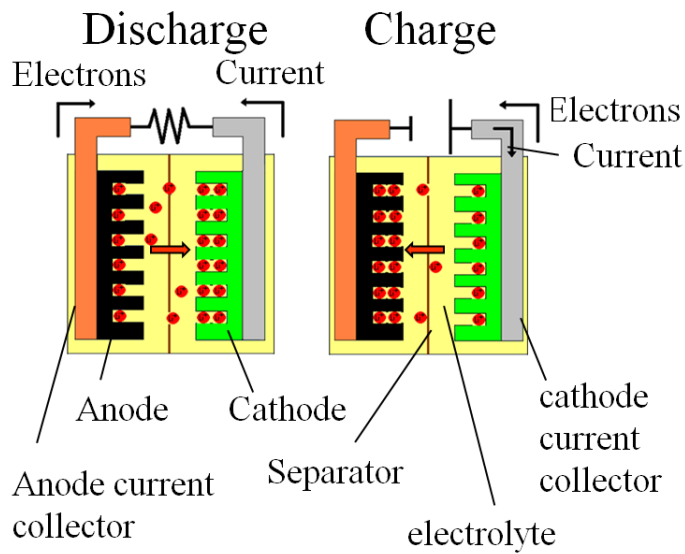


Figure 1 Schematic of charge and discharge processes that take place in a lithium Ion cell.

Battery Capacity

Over the life of a cell, physical phenomena contribute to degradation in the cell's performance. This drop in performance is most notably recognized in the decrease in capacity (capacity fade) which can occur during usage (charge and discharge cycling) or periods of rest (ageing effects influenced by time, temperature and state of charge). Capacity, expressed in Amp-hours, is defined as the available current a battery can supply over a given time period. It is a measure of electrical charge. Capacity can be measured directly during discharge by integrating current with respect to time:

$$Q = \int_{t_1}^{t_2} Idt$$

where Q is the measured capacity, I is the instantaneous discharge current, t_1 is the time at the beginning of the discharge period and t_2 is the time at the end of the discharge period. Capacity is used as a performance metric by manufacturers who assign a “rated capacity” to all their batteries. The rated capacity gives the amount of charge a new battery should be able to deliver when it is discharged from a fully charged state to a fully discharged state. If a battery is rated

1000mAh, it should be capable of continuously supplying 1000mA over a one-hour period. The current with which a battery is discharged is often expressed in terms of “C-rate.” This term describes the current normalized by the rated capacity:

$$Crate = \frac{I_{discharge}}{Q_{rated}}$$

Where $I_{discharge}$ is the discharge current and Q_{rated} is the rated capacity. When discharging a battery at half the rated capacity or at a C-rate of 0.5C the battery discharge time should be 1/(C-rate) or 2 hours. However, in reality this is often not the case for several reasons. First, when a manufacturer assembles a particular type of battery, there is a degree of uncertainty that can be associated with the materials and processes that will ultimately lead to slight variations in performance from battery to battery. However, manufacturers will typically only assign one rated capacity to an entire lot of batteries. Therefore, the rated capacity depicts a distribution of actual capacities. To describe the actual capacity measured from a fully charged state to a fully discharged state of one particular battery, this text will use the term Q_{max} .

Determining when a battery is in its fully charged or fully discharged state, or in general, the determination of state of charge (SOC) presents some unique challenges in itself that will be described later. For the purpose of explaining capacity, we will assume that SOC is a function of the battery’s open circuit voltage (OCV) or the voltage that is measured across a battery’s leads when there is no load placed on the battery. When the battery is fully charged the SOC is 100% and when the battery is fully discharged the SOC is 0%. Manufacturers often set a high and low operational voltage limit for their batteries which can be corresponded to a fully charged SOC and a fully discharged SOC respectively. These voltages are chosen based on both the operational requirements of the host device as well as stable voltage potential of the battery

materials. At large voltage levels the cathode can undergo decomposition and react with the electrolyte [10]. Therefore the cell voltage should never go above V_{\max} which describes the cell potential when it is in its fully charged state, or below V_{\min} which is the cell potential in its fully discharged state. Using this we can describe Q_{\max} as:

$$Q_{\max} = \int_{t_1}^{t_2} Idt$$

where

$$SOC(V(t_1)) = 100,$$

$$SOC(V(t_2)) = 0,$$

and

$$V(t_1) = V_{\max},$$

$$V(t_2) = V_{\min},$$

The second reason battery discharge time cannot always be accurately described by $1/(C\text{-rate})$ is that, Q_{\max} is dependent on C-rate [11]. This is a somewhat counterintuitive notion which suggests that the amount of charge that can be delivered by a battery is dependent on the rate at which the discharge current is delivered. Batteries supply less charge at higher current rates due to diffusion limited processes. During discharge, lithium ions can only be inserted into the cathode at a limited rate depending on the charge transfer resistance between the electrolyte and the electrode. Also, lithium diffusion through the porous separator can be a limiting factor at high current discharges depending on the separator pore size as well as the electrolytic resistance.

The relationship between Q_{\max} and the discharge current rate was first observed in lead acid batteries and was reported by Peukert in a paper in 1897 [12]. It has since been shown to be applicable to lithium ion batteries and suggests that a constant current discharge current to the k^{th}

power multiplied by the corresponding discharge time is a constant over a range of different currents. Therefore:

$$I_1^k t_1 = I_2^k t_2$$

where I_1 and t_1 are some discharge current and time, I_2 and t_2 are a known discharge current and its associated discharge time and k is Peukert's constant. From this relation we can derive the capacity of a battery when discharged at any constant current rate by:

$$Q_1 = Q_2 \left(\frac{I_2}{I_1} \right)^{k-1}$$

where Q_2 is a known Q_{max} when discharging at a current of I_2 and Q_1 is the Q_{max} in question for a discharge current of I_1 . This relation is derived in [13]. When this model is empirically fit to data, k is generally found to be greater than 1 due to the reduction of Q_{max} with an increase in discharge current I . A Peukert's constant of exactly 1 suggests that there is no loss in capacity with increasing current rate. Therefore, batteries that exhibit k values close to 1 are better at delivering high power with respect to their energy density.

The value of Q_{max} is influenced by the ambient operating temperature. A higher operating temperature enhances the kinetics of lithium diffusion allowing for easier transport of lithium ions between the anode and cathode. Because of this, a higher Q_{max} can be achieved by discharging at higher ambient temperatures. It should be noted that at a certain upper temperature threshold, failure mechanisms (melting of the separator, thermal decomposition of the electrolyte) can be induced which will ultimately lead to a hard battery failure so this relationship between temperature and capacity only exists at a certain temperature range.

Q_{max} is also time dependent, eventually declining with usage or with aging. This is known as capacity fade and the physical mechanisms that govern this behavior will be explained

in the “failure mechanisms” section of this paper. At the beginning of battery life, the measured Q_{\max} value should be close to the manufacturer’s Q_{rated} .

$$Q_{\max}(t) \approx Q_{\text{rated}} \text{ for } t=0$$

where t is time. However, Q_{\max} will ultimately decrease as the battery ages. The non-recoverable decrease in Q_{\max} with respect to the nominal capacity Q_{rated} can be used as a measure of state of health (SOH) by:

$$SOH(t) = \frac{Q_{\max}(t) - p(Q_{\text{rated}})}{Q_{\text{rated}} - p(Q_{\text{rated}})}$$

where p is a number from 0 to 1 describing the failure threshold of a battery in terms of the percent reduction of the Q_{rated} . Therefore if a battery is considered to be failed when its capacity degrades to 80% of its nominal capacity, then $p=0.8$.

Noting that the actual battery capacity depends on usage and environment, a problem arises when attempting to rate a battery’s capacity. Unless the rating method is standardized between all manufacturing companies, it is possible for two identical batteries to be assigned different rated capacities solely based on the discharge current, temperature, V_{\max} , and V_{\min} values used to test the battery. Standards set by groups such as the Institute of Electrical and Electronics Engineers (IEEE) and the International Electrotechnical Commission (IEC), suggest that manufacturers define the rated capacity based on internal specifications. IEEE maintains,

“Production cells shall pass the qualification tests at specified intervals that the manufacturer/supplier specifies to maintain compliance with the manufacturer’s/supplier’s internal specification. The manufacturer’s/supplier’s specifications and documentation shall be made available as appropriate under general business terms and conditions to verify control of this criteria or process... Important performance evaluation parameters include capacity, impedance, cycle life, dimensions, and voltage characteristics”

The IEC defines rated capacity as,

“Capacity value of a battery determined under specified conditions and declared by the manufacturer”

The ambiguity of these standards is somewhat necessary due to the fact that batteries are purposefully designed to meet different operational requirements. In cases such as cell phones and portable electronic devices, low current and high energy densities are required. This would lead to batteries being qualified using low current discharge tests. In applications such as power tools and hybrid vehicles, operating conditions will require large discharge currents and high temperatures and therefore qualification tests should match those high power operating conditions. This provides assurance to customers who deal directly with battery manufacturers and propose application specific designs so that the battery meets the requirements of the host device. However, in many situations, battery customers are not directly involved during the manufacturer’s design phase and instead must “shop” among many existing batteries in order to find the best power solution to fit their needs. In this sense using the rated capacity to compare different types of batteries can be misleading.

Table 1 shows a review of specification sheets from several different manufacturers. For most sheets the nominal capacity was given at a C-rate of 0.2C. In some cases the discharge voltage profiles were given under different C-rates up to 2C. In other cases discharge at different temperature profiles were shown. Many of the sheets also contain cycle life information showing the capacity fade under charge/discharge testing. However, it is rare to find data sheets which give sufficient information to characterize all the properties of a particular battery.

Considering an application that requires short bursts of high current, in a high temperature environment, if two batteries are being considered that have the same rated capacity measured at the same C-rate, it does not imply that they are equally qualified to fit the needs of the system. If the system load requires a 5C discharge, it is likely that the Q_{max} of the two batteries under a 5C discharge will be different even though they were rated the same under a 0.2C discharge. In order to better represent the capability of batteries under different load

conditions, manufacturers could report on the Peukert's constant (k) of their batteries. This would give the user a better idea of how well a particular battery can handle high power applications.

Company	Rated Capacity	current used for rated
Power Source Energy Co , Ltd.	530mAh	.2C or 106mA
Xtra-Power	550mAh	.2C or 110mA
Shenzhen BAK Technology Co. Ltd	500mAh	.2C or 100mA
BYD Battery CO., LTD	750mAh	.2C or 150mA
Heter electronics group (LiFePO4)	3200mAh	.5C or 1600mA
LionikBattery Co.,Ltd	850mAh	.2C or 170mA
UltraLife	900 mAh	.2C or 180mA
PowerStream	1250mAh	.5C or 575mA

Table 1 Review of Specification Sheets from Several Battery Manufacturers

Another consideration which can't be deduced from the rated capacity is the cycle life. The rated capacity gives information as to how much charge can be delivered during one particular cycle at one discharge rate, but the amount of charge a battery can deliver over its entire lifetime is another important factor. As mentioned, some data sheets report on the capacity fade however, this information is only given at one discharge condition. It is widely known that cell cycle life can be reduced with increasing temperature or increasing discharge current [14,15]. Therefore it is important to understand how cycle life will be affected during operating conditions so that a battery can be chosen that will best deliver energy over the course of its life.

In Figure 2 Q_{\max} vs cycle number (capacity fade curve) is plotted for 2 batteries, "A" and "2A". Battery "A" was rated 0.9Ah and cycled at a C-rate of 0.5C corresponding to a discharge current of 0.45A. Battery "A2" was rated 0.53Ah and cycled with a discharge C-rate of 1C. From Figure 2 and as documented by their manufactures, battery "A" at the beginning of life has a higher capacity than "2A." This was mostly due to the fact that battery "A" was larger, and had a higher mass of active material making up its electrodes. However, we see that the rate of capacity fade of battery "A" is much faster than "2A." In this figure we assume that the failure

threshold is marked by a 20% reduction of the rated capacity and each failure threshold is shown by a blue line. It can be seen that battery “A” reaches failure just around 200 cycles while battery “2A” lasts over 600 cycles even while supplying a higher discharge current than battery “A.” If the Q_{max} values are summed up over every cycle from the beginning to the end of life, we find that battery “A” delivers a lifetime capacity of 155.5Ah while battery “2A” delivers a lifetime capacity of 293.9Ah. Thus when considering these two batteries, if the application requirements during a single use can be filled by “2A” then it makes more sense to use this battery as more energy can be delivered over the life time of the battery. However, if a single use application requires a charge to be delivered at more than 0.53Ah, battery “2A” would not be suitable and battery “A” should be chosen.

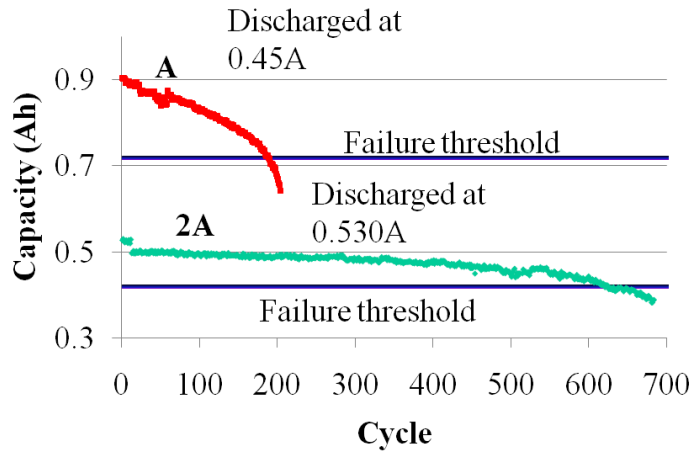


Figure 2 Capacity fade curves for two batteries with different cycle life properties

Failure Mechanisms

1.1 Internal Factors

Several mechanisms of capacity fade in Li-ion cells have been well defined in literature [2,16,17,18,19,20]. Such degradation has been attributed to the following:

- Breakdown of the electrolyte's organic solvents and salts
- Chemical breakdown of active material in the electrodes due to side reactions
- Consumption of cyclable lithium due to side reactions
- Co-insertion of electrolyte solvents into the composite electrodes
- Increased impedance within the battery from build-up of surface films on the electrodes
- Delamination of the electrode from the current collector
- Electronic isolation of active material from the electrolyte
- Reduced coherence between particles making up the composite electrodes
- Separator shrinkage or melting
- Internal short circuits from impurities or dendrite growth
- Cracked or broken leads

The first four mechanisms mentioned above, breakdown of the electrolyte solvents and salts, chemical breakdown of the electrode materials, consumption of lithium, and co-insertion of organic solvents into the electrodes, play an important role in the fifth mechanism mentioned, the increase in surface film thickness. This surface film, often called the solid electrolyte interface (SEI) is widely recognized as a major contributor to increased internal resistance and over all cell degradation. The actual composition of the SEI is highly complex and layered. It is composed of products from side reactions between the electrolyte, electrodes, and lithium.

Li-ion cells are assembled in a discharged state [1]. At this point, all cyclable lithium ions are contained within the cathode and migration though the electrolyte has not yet occurred.

During the first charge, or the “formation period,” lithium ions move thought the electrolyte and, in the process, initiate several chemical side reactions (see Figure 3). At potentials below 1.5V, reductions of alkyl carbonate molecules and salt ions such as PF_6^- begin to form insoluble Li salts, which adhere to the carbon anode [2, 16]. The buildup of precipitates over the course of the first charge eventually forms a stable surface film on the anode known as the solid electrolyte interface or SEI. The initial formation of the SEI layer consumes a considerable portion of lithium ions in irreversible reactions. This material can no longer be cycled within the cell; thus, in order to maintain a working capacity balance, the cathode is assembled with up to 14% excess capacity [2] in order to account for the formation of the SEI layer. The formation period is a critical step in determining the overall health of the battery and is usually performed by the manufacturer under specific charge conditions before the battery is put on the market.

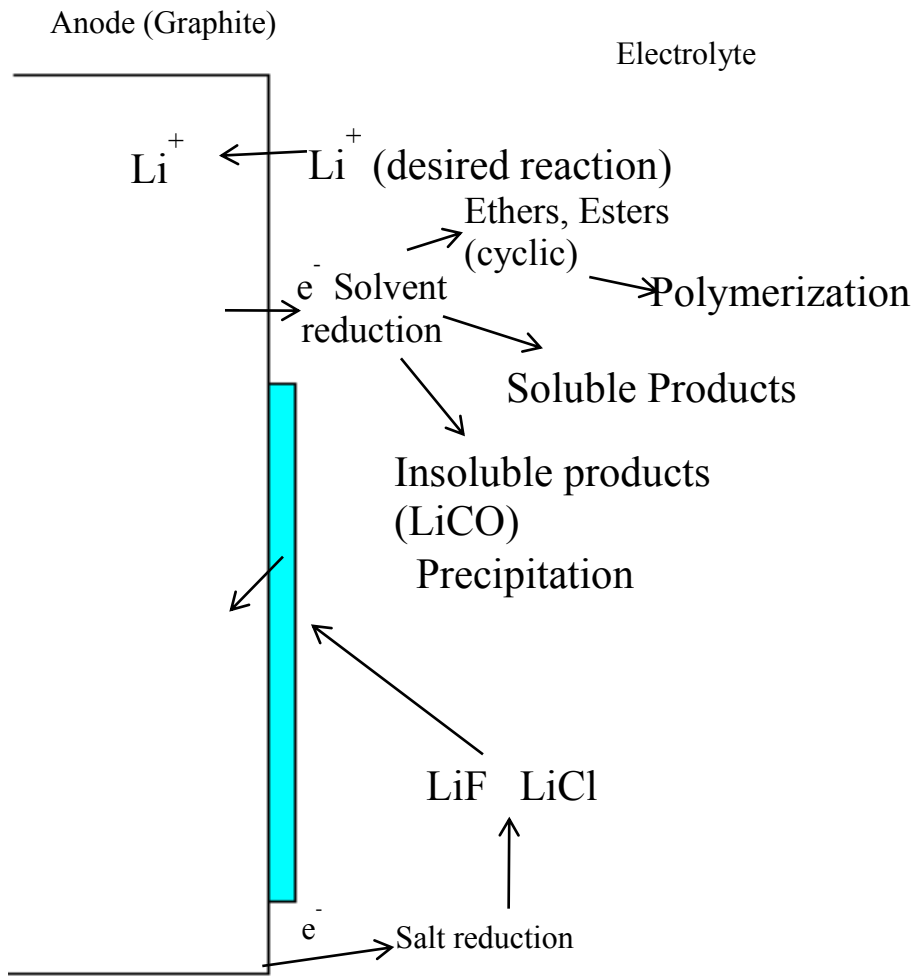


Figure 3 Schematic of side reactions that take place at the anode electrolyte interface [2]

An ideal SEI layer provides adequate Li^+ transport, insulates electrons, and isolates the anode from the electrolyte to prevent further reduction of electrolyte components. Continuous cycling and storage of cells begins to change the composition and increase the resistance of the SEI layer. This change occurs from the stresses incurred by anode expansion during lithiation. The carbon anode is made of multiple layers of graphite, and during charging, lithium ions are inserted between these layers increasing the lattice volume [21]. The expansion of the anode causes cracks in the SEI layer, which are repaired by further reduction of the electrolyte on the carbon anode during solvent co-insertion. Solvent co-insertion refers to when components of the electrolyte are simultaneously inserted into the electrodes with lithium. This crack and repair cycle not only

increases the thickness and resistance of the SEI layer, but it also consumes lithium ions which further reduces capacity [18]. This process is illustrated in Figure 4. Additives such as vinylene carbonate (VC) have been shown to increase cycle performance by promoting thin and dense SEIs that help suppress solvent reduction [22].

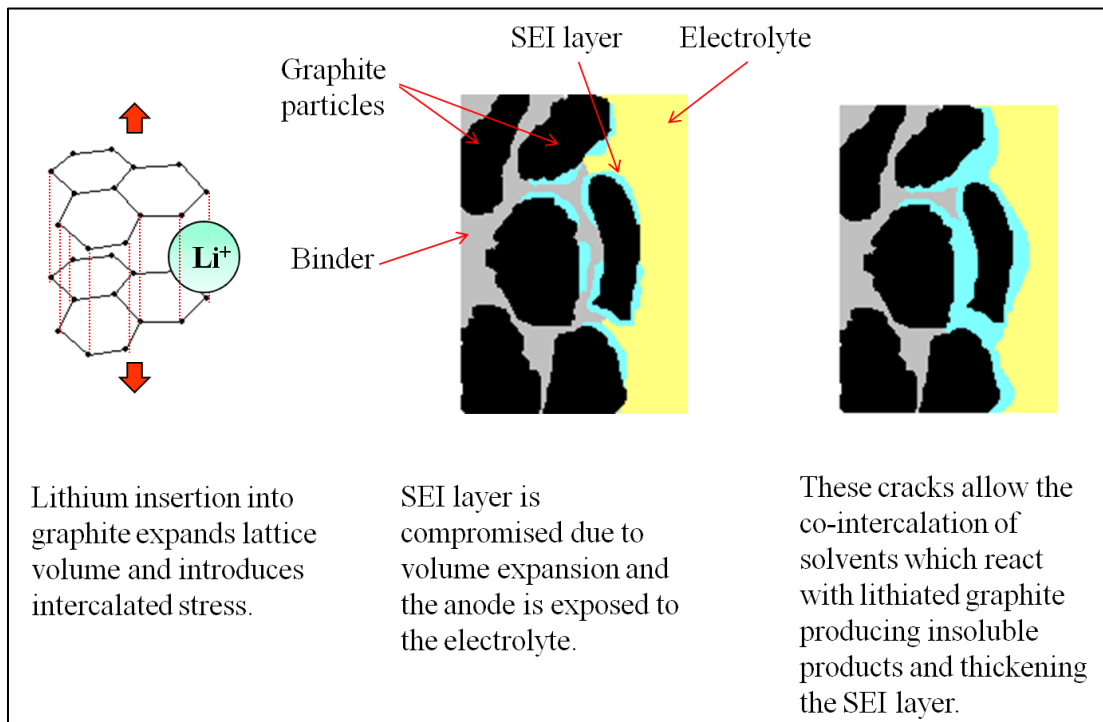


Figure 4 Processes of surface film thickening from lithium insertion

The electrode expansion and contraction responsible for the increased thickness of the SEI layer can have other negative effects on battery performance. If the expansion of the electrodes is large enough to break the bond between the electrode and the current collector, delamination can occur. The current collector is the substrate on which the electrodes are deposited and it provides the conductive pathway for electrons to flow from the electrodes out to the device that the battery is powering. However the current collector is not capable of lithium insertion and therefore does not expand and contract during charge and discharge cycles which, leads to interfacial stresses between the anode and the current collector. If delamination occurs,

there are less contact points between the electrode and the current collector which can raise the internal resistance in the battery and possibly cause current crowding at the interface.

Global expansion and contraction of the electrodes can also result in poor local cohesion of the electrode particles themselves. This presents a problem because a majority of the electrochemical activity within the battery occurs at the surface of the electrodes that are exposed to the electrolyte. In order for the current facilitated by these reactions to move through the current collector and out to the external leads, electrons must first travel from the surface through the thickness of the electrodes. This is why a conductive additive (usually graphite) is added to the composite cathode electrode. However, if cohesion between the electrode particles is reduced the proximity of neighboring particles in the bulk electrode decreases. This increases the resistance in the bulk electrode and the overall resistance in the cell. Likewise if parts of the electrode crack and become electrically isolated from the bulk electrode, these pieces of active material can no longer transfer energy to the current collector, actively reducing the capacity of the battery. It should be noted that the scale of these types of phenomena are much smaller in size than that of the whole electrode and will often occur in localized regions. Therefore this phenomenon may result in a subtle contribution to the total cell degradation.

Independent of the electrodes, battery degradation can occur due to the polymer separator. The function of the separator is to maintain electrical isolation between the anode and cathode to prevent internal short circuits while allowing the electrolyte and lithium ions to easily flow between the electrodes. Polymer separators can undergo thermal shrinkage during high temperature applications [23] reducing the isolation coverage between the anode and cathode. The shrinkage occurs when the polymer separator swells at high temperatures and closes off the separator's porous gaps. The reduction in pore size reduces the overall coverage area of the separator because the swelling fills in the interstitial gaps of the separator film (rather than expanding outward). Reduction in pore size also limits the kinetics of lithium ions diffusing

though the separator resulting in a reduction of the battery's ability to deliver high current rates. At extremely high temperatures, it is possible for the separator to melt completely and allow the anode and the cathode to make contact. This would result in an internal short circuit causing rapid discharge and further heat generation leading to a hard failure in the battery.

Separator failure may also occur due to a tear or puncture. This could be caused if the cell undergoes a sudden mechanical load and a compressive force pushes the electrodes through the separator. Another major concern is the formation of dendrites on the electrode surfaces which can puncture the separator and cause an internal short. Dendrite formation is a major concern with cells that use lithium metal as an anode; hence commercial lithium ion batteries typically use graphite as the negative electrode. However, it has been found that due to the slow kinetic processes during low temperature charging, lithium plating on the surface of the graphite anode can occur. If this lithium plating is not allowed to diffuse back into the electrolyte during discharge, dendrites may form. Internal shorts may also occur due to impurities introduced on the electrode surface during manufacturing.

1.2 External factors

There are many external factors that influence the performance and life of a lithium ion battery. Several studies have been conducted on the influence of ambient temperature. Generally, Li-ion batteries can be made to perform well at temperatures ranging from -30 to +40°C [17]. Elevated temperatures usually help to facilitate ion diffusion, which can initially increase cell capacity. However, added heat also speeds up side reactions which contributes to the thickening of the SEI layer and reduces the overall cycle life of the cell [24, 17]. A decrease in ambient temperature has the opposite effect, hindering ion diffusion and greatly reducing discharge capacity. During storage, when the battery is not in use, low temperatures correlate to longer shelf lives and preservation of cycle performance [25].

Profiles that govern the charge or discharge cut off voltages also affect the life of secondary cells. Manufacturer recommendations often specify batteries to be charged for a specific amount of time employing the constant current constant voltage protocol to allow for sufficient lithium intercalation into the anode. Upon discharge,⁺ batteries supply current until they have reached a specified cut-off voltage prescribed by the manufacturer. The maximum/minimum allowed voltages that a battery may be charged/discharged to, are usually governed by a circuit contained within the host device. This circuit is usually part of a larger battery management system (BMS). These predetermined cut-off voltages set by the manufacturer provide optimal battery performance and lifetime. Additionally, a simple safety circuit is attached to the battery's terminals to provide protection by restricting current flow and cutting off power if a maximum or minimum safety voltage is reached within the battery. The safety circuit is designed more to protect the battery from undesirable thermal conditions rather than govern the charging profile of the cell.

Uncontrolled charge profiles can lead to over-charging where excessive voltage levels introduce heat and accelerate breakdown of the cathode and electrolyte resulting in gaseous byproducts to build up in the outer casing. Cut-off voltages that are set too low put excess stress on a cell during discharge by prompting anode decomposition. There are several reasons why the voltage considerations recommended by the manufacturer are not followed. In systems containing multi-celled battery packs, where several cells are connected in series or parallel, one cell may degrade slightly faster than the other cells over numerous charge/discharge cycles, resulting in it having a different state of charge than the cells surrounding it. Therefore, during charging or discharging this "out of phase cell" may be forced into a deep discharge or over-charge during usage (because each cell experiences the same current during charging). This is known as cell mismatch and many BMSs attempt to correct this by re-aligning the state of charge of each battery in a battery pack. This can be accomplished by distributing charge so that cells with a higher charge, give their charge to cells with a lower charge, effectively balancing the battery

pack. A defect in the battery's safety cut-off circuit could also result in overcharging if the battery is left to charge for an extended period of time and the safety circuit fails to shut off the charging current. Figure 5 shows images taken upon visual inspection of a safety cut-off circuit. Figure 5(a) shows solder bridging taking place across a MoSFET device and Figure 5(b) shows evidence of stray solder bridging the thickness of the substrate.

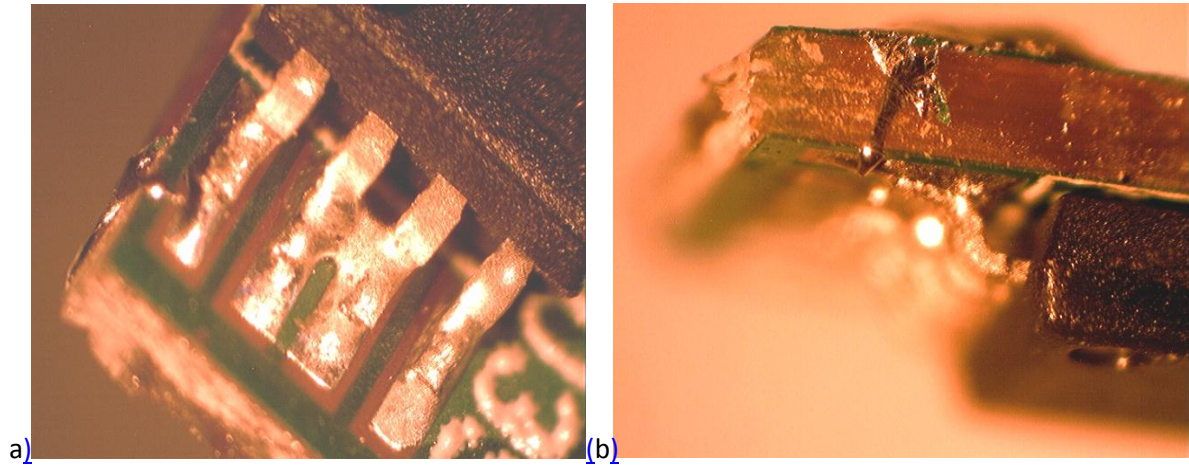


Figure 5 A malfunction in a battery's safety circuit could give way to abnormal cycling profiles. This figure shows images taken upon visual inspection of a safety cut-off circuit. In part (a) there is an example of solder bridging taking place on a MOSFET device and in part (b). bits of stray solder were found wrapping around the substrate.

Battery reliability can also be affected by the current profile applied to the battery. High current levels both during charging and discharging are typically associated with a faster rate of capacity fade. This is due to the higher temperatures associated with larger currents moving through the cell as well as the faster thickening of the SEI layer [11]. Also, parameters in the charging protocol such as the current termination point which specifies the cut-off current that marks the end of the constant voltage charging mode have been shown to affect reliability. Lowering this cut-off current may increase the immediate discharge capacity of the cell but could negatively affect the cell's cycle life.

In order to examine degradation and failure of lithium ion batteries, it is sometimes necessary to directly examine the anode, cathode and separator. This requires dissassembly of the the

battery. In reviewing the literature, limited information was provided. This following section provides a review of existing material as well as procedures developed for this thesis.

2. Failure analysis of Lithium Ion batteries

Electroanalytical techniques such as electrochemical impedance spectroscopy (EIS) and cyclic voltammetry can be used to infer how degradation mechanisms progress and the sites where they arise. However, due to the number of complex and often competing mechanisms that govern battery degradation, it is possible for electroanalytical techniques to be interpreted in different ways. In order to directly examine the internal conditions of a battery, a systematic disassembly must be performed.

Once a battery is assembled, it undergoes electrochemical processes that advance during usage. Thus, a lithium-ion battery will never have the same chemical makeup at any two points in its lifetime. The negative electrode, which begins as a stable graphite powder during assembly, is coated in a porous surface film of mostly inorganic compounds upon contact with the electrolyte. During the first charge cycle, at voltages above 0.15V [26], this film evolves into a compact highly conductive layer known as the solid electrolyte interface (SEI), while lithium ions are intercalated into the graphite anode forming LiC_6 . In the cathode, lithium is lost during charging, and decomposition reactions occur with increasing voltage. Further cycling leads to alterations in the lattice structure and the formation of nonconductive films that hinder ion diffusion and increase charge transfer resistance [27]. Solid precipitates, which are the main contributors to electrode surface films, form during reduction of the electrolyte. Break-down of the electrolyte's organic solvents releases gaseous byproducts that increase internal pressure and alter the chemical atmosphere within the cell. Once a cell has undergone these physio-chemical changes, new considerations that are different than what was assumed during assembly must be made in order to safely and effectively disassemble a battery.

Currently, there are no standards or methodologies for conducting lithium-ion battery disassembly, but IEEE 1625 [28], “Standard for Rechargeable Batteries for Multi-Cell Mobile Computing Devices,” notes that to conduct disassembly:

“...a specialized, highly trained operator is essential. Additionally, the disassembly portion of this test shall be carried out in a controlled environment, such as a purged glove box.”

In several studies [29,30,31] electrode surface analysis has been performed on disassembled cells. Surface analysis has including scanning electron microscopy, X-ray diffraction, energy dispersive spectroscopy, and atomic force microscopy. However, the only details regarding disassembly in these papers were that disassembly was carefully conducted with discharged cells in an argon-filled glove box.

The most detailed disassembly process has been reported by Aurbach. In this study [32], carefully planned steps were documented to create a safe and repeatable process for removing active material from a cell’s outer casing. Fig. 6 shows Aurbach’s homemade mechanical cutting system customized for 18650-type batteries. This system was mounted inside of a glove box (the environmental conditions of this particular glove box were not mentioned) and controlled remotely by an operator. The bottom stage was moveable in the x and y directions and an electric motor and gear system were used to rotate the clamp sleeve holding the battery. A carbide-tipped saw was applied while rotating the battery in order to remove the cap of the battery case. A cut was made along the z direction of the case so that the electrodes could be easily removed. The electrodes were then removed from their original glove box and transferred to a highly controlled glove box with a pure argon atmosphere and water and oxygen contents ranging from 2–5 and 5–

10 ppm respectively. This procedure eliminated the safety hazards of close user contact with the cell during disassembly, but it was only applicable for standard-sized cylindrical cells.

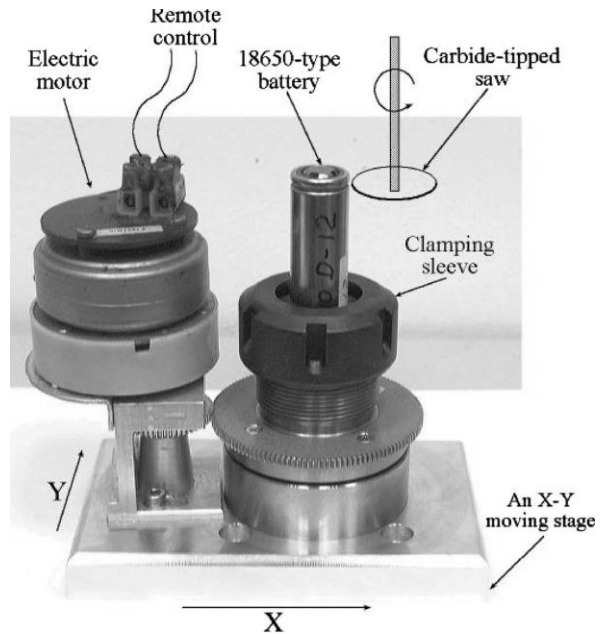


Fig. 6 Homemade cutting system [32]

Swart and Mikolajczak [33,34] have documented several destructive and non-destructive procedures to investigate the root cause of battery failure while minimizing post-failure defects. They mention that X-ray analysis should be used for guidance before disassembly to avoid damaging critical components in the battery. Mikolajczak et al. [34] found that a cell can be removed from its casing and then the electrodes can be unrolled or separated depending on the cell's wound or stacked configurations. These references, however, do not mention the type of atmosphere that disassemblies should be conducted in.

To provide the motivation for battery disassembly, a review of failure analysis and its connection to battery disassembly is discussed. Because batteries may contain potentially dangerous materials, safety hazards and precautionary measures are reviewed. This section is followed by environmental considerations that should be taken into consideration when a battery is disassembled. Lastly, a detailed procedure for disassembling a prismatic lithium-ion cell is given.

Review of Failure Analysis

The purpose of any failure analysis is to identify the location(s) of a failure and the fundamental (root cause) mechanisms that caused the failure. In the case of lithium-ion batteries, failure can be defined as a sudden loss of performance that can be attributed to a number of different causes. These can include an internal short circuit between electrodes, disconnection of the terminal tabs from the cell, or decomposition of active material due to excessive over-charging. In addition, under normal operating conditions, failure can also be defined in terms of degradation processes that advance beyond a threshold of acceptable use. Batteries are closed systems, hermetically sealed to prevent unintended side reactions with outside agents. Thus direct isolation of the failure site or effective diagnosis of failure cannot be conducted until a battery is ready to be permanently removed from operation.

Non-Destructive Failure Analysis

There are several indirect methods available which do not require disassembly that can be used during a battery's lifetime to measure degradation; an increase in internal DC resistance or a decrease in power output are examples [35, 36]. The resistance can be determined by measuring the current and voltage at two different current pulses by [37]:

$$R = \frac{V_2 - V_1}{I_2 - I_1} \quad 1.$$

where I_1 and V_1 are the current and voltage values at the first pulse and I_2 and V_2 are the current and voltage values at the second pulse. However, resistance has been shown to display some unpredictable characteristics during cycling and is therefore not typically used as the sole indicator of degradation. A decline in capacity (capacity fade) is a more common metric for battery degradation. Capacity fade describes the amount of charge a battery can store at any point in its life-time. Capacity, in ampere-hours (Ah), can be calculated by collecting current and time data during operation and using the relationship:

$$\text{Capacity}(Ah) = \int Idt \quad 2.$$

where I is the discharge current in amperes (A) and t is the time in hours. If capacity is evaluated from the battery's fully charged state to the fully discharged state, then it will give the maximum capacity or the total amount of charge the battery is capable of holding. As a battery is aged or undergoes charge/discharge cycling, the maximum capacity will decrease to a point in which the battery is considered failed and should be replaced. While capacity fade and DC resistance provide quantitative measures of battery degradation, they do not give any insight into the internal degradation mechanisms and how they each contribute to the loss of performance.

Electrochemical impedance spectroscopy (EIS) has been used as a non-destructive method to monitor degradation [32,38,39]. This technique measures the internal impedance of a battery over a range of frequencies. In most EIS systems the frequency ranges from a few millihertz to the megahertz ranges. These data are interpreted by means of a Nyquist plot where the real

values of impedance are plotted versus the imaginary values of impedance. A Nyquist plot for a typical battery resembles a semi-circle with a tail, as shown on the right side of Fig. 7.

By matching the Nyquist plot of an electrochemical system to that of a resistor-capacitor system, an equivalent circuit model can be derived. A resistor in series with a capacitor and a resistor in parallel produce a perfect semi-circle Nyquist response, which is considered the simplest form of an electrochemical equivalent circuit (shown on the left side of Fig. 7). The simple equivalent circuit acts as a starting point for building more complex models that represent the dynamic response of a battery. More complex models may include components that simulate non-faradic battery processes, varying electrode geometries, or diffusion-controlled processes, namely, the Warburg impedance [40].

EIS serves two important functions. Firstly, it can be used to predict a battery's electrical response under different discharge conditions, as in [41]. This is accomplished by extracting the resistance and capacitance values of the equivalent circuit components from the EIS data generated by a battery. Then, the equivalent circuit can be evaluated at different voltage or current inputs using traditional circuit analysis.

EIS can also be used as a non-destructive failure analysis tool. Non-destructive analysis requires a physical interpretation of the electronic components in the equivalent circuit. Fig. 7 shows a common interpretation of the simple equivalent circuit where the first resistor " R_p " is considered to be the resistance of the electrolyte and C_{dl} and R_{ct} are considered to model the electrode interface. By correlating each component to a degradation site and corresponding degradation mechanism, the contributions of each root cause can be identified by monitoring the changes in the equivalent circuit's components over a battery's lifetime. The value of R_p is equal to the real value of impedance where the Nyquist plot first intersects the x-axis. Therefore, EIS data

generated over a battery's cycle life which shows the Nyquist plot shifting towards the right indicates an increase in the value of R_p . Because this value is associated with the electrolyte, an increase in R_p can be interpreted as a chemical breakdown of electrolyte solvents or lithium salts. The second resistor R_{ct} is the charge transfer resistance and is equal to the diameter of the semi-circle produced in the Nyquist plot. This value is affected by how readily lithium ions are inserted into the electrodes. The rate of lithium insertion is determined by properties such as the porosity of the electrodes and the growth of surface films. When EIS data confirm an increase in the value of R_{ct} , increased resistance due to surface films or a decrease in lithium insertion sites can be assumed. The capacitor in the equivalent circuit C_{dl} is the double-layer capacitance and is influenced by the capacitive properties of the cell. The interface between the electrodes and the electrolyte has a capacitive component which is influenced by the growth of surface films. There may also be capacitive components observed between individual electrode particles or at the interface between the electrodes and the current collectors. An increase in C_{dl} may indicate a change in the capacitive properties of the surface films, delamination of the electrodes from their current collectors, or lack of cohesion of electrode particles.

The use of EIS as a non-destructive failure analysis tool was demonstrated in [42] on a lithium oxide battery. The equivalent circuit model in this study was constructed such that separate electrical components were used for the interface and the electrodes to help distinguish between different degradation sites. EIS measurements were taken at different times between 1 and 20 cycles to show how the electrical properties in different parts of the battery changed with usage.

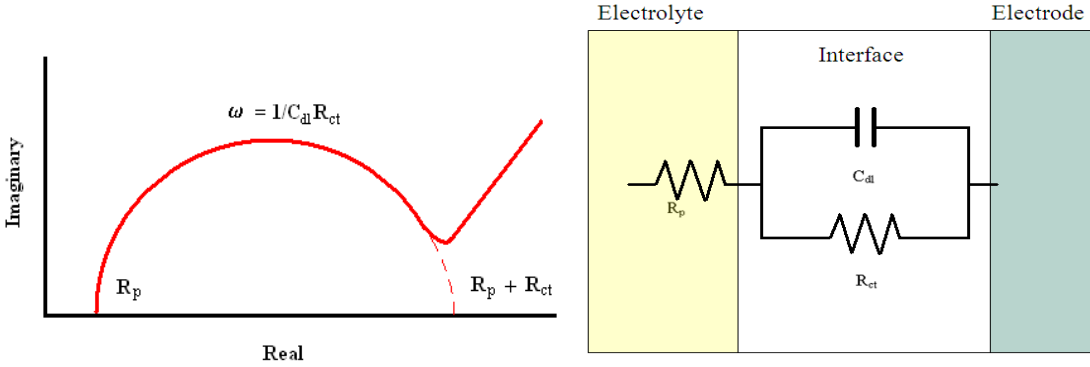


Fig. 7 Simple equivalent circuit for an electrochemical system and corresponding Nyquist plot

Chemistry-dependent (physics-of-failure) methods [43] have been proposed for measuring degradation. Zhang [44] produced cyclic voltammograms of Sony US18650S cells before and after cycling and found a decrease in the peak currents with increasing cycle number. Chen [45] outlined a cyclic reciprocal derivation chronopotentiometric method in which peak heights of $dI/dE-E$ curves were related to adsorption, deposition, and corrosion processes. In lead acid batteries, chemistry-dependent methods have been used for online state estimation. Baert related noise in a measured voltage signal to discharge-diffusion homogeneous reactions and discharge-adsorption reactions [46]. As a battery degrades, the reaction rates change accompanied by a higher degree of noise in the voltage signal. This can be used to monitor the amount of degradation. The “coup de fouet,” which is the voltage drop observed at the beginning of discharge in lead acid batteries, has been related to crystallization overvoltage [47]. The peak of this voltage drop was found to have a linear relationship with capacity.

Voltammograms similar to those described by Zhang are shown in Fig. 8. We conducted cyclic voltammetry by applying a linear voltage sweep from 3V to 4.2V at a ramp voltage of 0.1mV/sec

for two lithium ion batteries obtained from the same manufacturer. A small ramp voltage was chosen to negate the capacitive effects at the interface of the electrode and electrolyte. At the time the voltammograms were obtained, battery 1 had undergone a single charge/discharge cycle and displayed a capacity of 0.63 Ah, while battery 2 had undergone 950 cycles and had a capacity of 0.55Ah. During the forward voltage sweep of battery 1, the current began to increase at a high rate around 3.7V. This increase indicates the point at which the electrodes reach their reduction potentials and electrons are lost at the cathode and gained at the anode. The current reached a maxim at just over 4V and then began to decrease due to the depletion of lithium available for charging. When the potential reached 4.2V, the ramp voltage was inverted and the process was reversed. During the discharge, the peak current was observed at a voltage of around 3.6V. Battery 2 produced a voltammogram similar to battery 1; however, the peak currents were slightly lower and occurred at lower potentials due to extended charge/discharge cycling. This suggests the consumption of lithium during side reactions and/or the reduced ability of the electrodes to store lithium due to surface films or the breakdown of the storage material.

Cyclic voltammetry offers a chemistry-dependent method to evaluate battery degradation while leaving the cell construction intact. However, peak currents are dependent on the voltage sweep rate, and in order to minimize capacitive influences on the current profile, the voltage sweep rate must be minimized. Therefore, creating voltammograms is not a quick check, as compared to the “coup de fouet” in lead acid batteries. Furthermore, the profile in Fig. 8 shows a relaxation of the current during the forward sweep at around 3.8V before the maximum current was reached. Voltammogram profiles such as these can be indicative of complex species interactions within the cell but specific information about these interactions can't be determined by cyclic voltammetry alone.

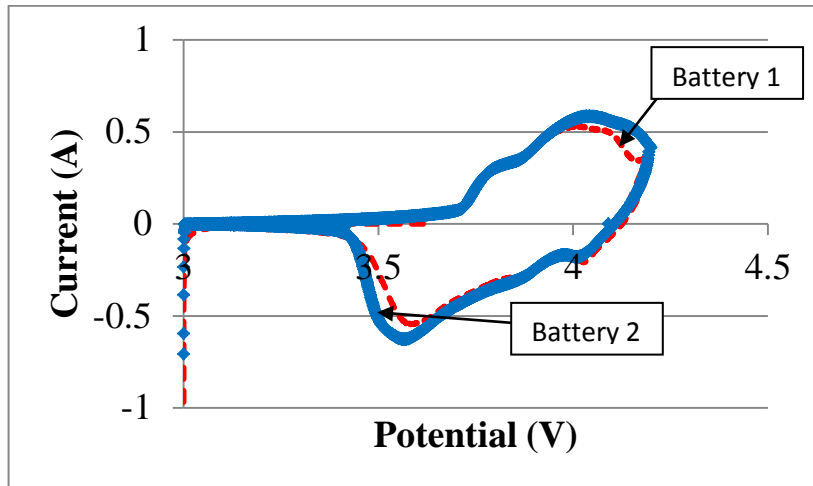


Fig. 8 Cyclic voltammograms for two batteries.

Transmission X-ray analysis and computed tomography (CT) scans are qualitative tools for non-destructive failure analysis. These techniques provide the only means to visually inspect the internal components of a cell without disassembly. From X-ray inspection, as shown in Fig. 9, internal shorts, cracks in the electrodes, and volume expansion from gas generation may be observed.

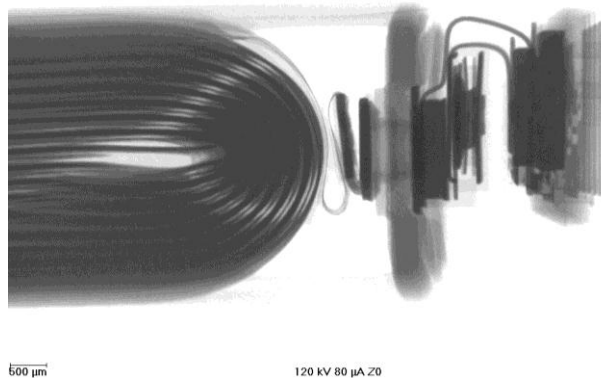


Fig. 9 X-ray image showing cell connections to the safety circuit and external terminals for a healthy battery.

Destructive Failure Analysis

Disassembly is necessary to observe and analyze the internal battery materials. Disassembly also provides a deeper insight into the individual sites that may be responsible for degradation observed at the cell level. Non-destructive failure analysis techniques, by contrast, are used to monitor battery performance during usage. However, the information gained is limited to inferences based on the electrical properties of the battery or to the X-ray images, which give little quantitative information.

Electrodes

A disadvantage of non-destructive analysis of Li-ion batteries is that it is difficult to determine the contribution of degradation from each individual electrode. One way this has been resolved is through the “reconstruction method,” where cycled cells are disassembled and then rebuilt using a degraded electrode and a new reference electrode. This method was demonstrated by Aurbach [32]. The reconstruction method was used to perform cyclic voltammetry and EIS on individual electrodes after cycling. The authors also constructed cells with non-cycled electrode materials to observe the effects of cycling on cell kinetics. These tests indicated sluggish ion transport due to surface films on both of the cycled electrodes. Itou [48] used the reconstruction method to investigate the sites of resistance increase in $\text{Li}_{1-x}\text{Ni}_{0.8}\text{Co}_{0.15}\text{Al}_{0.05}\text{O}_2$ cells. The authors compared the internal resistance of reconstructed coin cells using one of the cycled electrodes with a metallic lithium reference electrode and found that the cathode was responsible for the majority of resistance increase. Ramadass [29] reconstructed t-cells from cycled Sony US18650S batteries using lithium foil as a reference electrode. The authors applied low discharge current rates to the rebuilt cells (8mA/g for the cathode and 12mA/g for the anode) in order to calculate the cell

discharge capacity. This was conducted with cells removed from testing at different charge/discharge cycles to determine how the specific capacity of each electrode decreased with usage. The authors found a 17% decrease in capacity of the cathode after 800 cycles at room temperature and a 20% decrease in capacity of the anode after 800 cycles at room temperature.

Material characterization techniques can provide useful information when analyzing disassembled electrode samples. In the previously discussed paper, Aurbach [32] collected powder scraps from each electrode to perform powder X-ray diffraction (XRD). The author found a slight decrease in the XRD peak intensity after cycling, which suggested material degradation in both electrodes. The author also discovered characteristics peaks of graphite within the LiCoO_2 cathode. Because graphite was not found in non-cycled cathodes, it was suggested that the migration of charged graphite particles to the cathode could be one possible mechanism of self-discharge.

Itou's [48] results on electrode resistance increase were supplemented by investigating the morphology of a $\text{Li}_{1-x}\text{Ni}_{0.8}\text{Co}_{0.15}\text{Al}_{0.05}\text{O}_2$ cathode. Using a focused ion beam (FIB), Ga-ions were irradiated on the sample to cut cross-sections in the cathode. By observing the cross-sections with a scanning electron microscope (SEM), grain boundaries were observed. Cracking at grain boundary interfaces was found in the cycled samples. Changes in the lattice structure during charging were observed by XRD. Analysis of XRD peaks indicated a volume increase during lithium insertion, which provides the mechanism for electrode cracking during charge/discharge cycling.

Ramadass [29] performed XRD studies on electrodes that were cycled at different temperatures to evaluate thermal effects on electrode degradation. In this study, there were no significant changes in either the intensities or peak positions of the negative electrode, even between batteries cycled

at different ambient temperature conditions. This result suggested that there were no significant phase changes or degradation in the graphite electrode during cycling. In the cathode, Ramadass's [29] results were similar to those of Aurbach [32] in that there was a slight decrease observed in peak intensity with cycling. More specifically, the decrease of the (0 0 3) peak indicated the disorder of Li and Co cations in the octahedral sites of well-layered LiCoO_2 , which leads to areas of inactive lithium insertion.

XRD is commonly applied for material characterization in battery research, as seen in the previously mentioned works of Aurbach [32], Itou [48], and Ramadass[29]. However, other methods have been adopted by researchers such as Wu [49], who used Fourier-transform infrared spectroscopy (FTIR) to identify the components of an SEI layer as it evolved on a $\text{Li}_{1.05}\text{Mn}_{1.96}\text{O}_4$ cathode. In Wu's work, the batteries were cycled and then disassembled. Samples were prepared by grinding the cathode material into a powder and then pressing the powder into translucent pellets. From these pellet samples, FTIR absorption bands were found that corresponded to R- CO_3Li (R=methyl, ethyl) and Li_2CO_3 . The author concluded that these were products formed from the decomposition of the electrolyte (LiPF_6 salt and ethylene carbonate/diethyl carbonate solvents) and that they had existed on the cathode as surface films.

The SEI composition on the surface of carbon-based anodes was investigated by Peled [50] using X-ray photoelectron spectroscopy (XPS) and time of flight secondary ion mass spectrometry (ToF-SIMS). His test matrix included three different carbon substrates, namely, highly ordered pyrolytic graphite, hard carbon, and soft carbon, and three different electrolytes, including LiAsF_6 , LiTFSI , and LiPF_6 . XPS and ToF-SIMS results both confirmed the presence of a high concentration of LiF (from electrolyte salt reduction) on the cross-sectional plane of the highly ordered pyrolytic graphite; there was also a high concentration of organic polymers (from electrolyte solvent reduction) along the basal plane for all three electrolytes. Carbonates were

found in the cross-sectional plane of the highly ordered graphite and on the hard carbon substrate for the LiAsF₆ electrolyte. For the LiPF₆ electrolyte, carbonates were only found in the basal plane of the highly ordered graphite. The soft carbon electrode contained surface films consisting of LiF and other salt reduction products as well as organic material, but did not contain any carbonates for any of the mentioned electrolytes.

Kostecki [30] cycled pouched cells with LiNi_{0.8}Co_{0.15}Al_{0.05}O₂ composite cathodes and performed surface analysis via Raman microscopy. Focus was placed on three bands in the Raman spectra that were characteristic of LiNi_{0.8}Co_{0.15}Al_{0.05}O₂, acetylene black, and graphite; the latter two were added to the cathode as conductive agents. Many Raman spectra were taken over the surface of the cathode, which were analyzed and displayed as a color-coded mapping of the three mentioned bands. The results showed a non-uniform distribution of the cathode materials with concentrated clusters of LiNi_{0.8}Co_{0.15}Al_{0.05}O₂ and acetylene black on the cathode surface. Further Raman spectroscopy was performed on three different LiNi_{0.8}Co_{0.15}Al_{0.05}O₂ regions. A change in band width and peak intensity ratio was noticed and was attributed to the amount of lithium contained within the lattice structure. This indicated non-uniformity of charged particles throughout the surface of the cathode.

Other studies on failure analysis have investigated physical attributes of battery electrodes rather than specific material properties. In cases such as these, SEM analysis is helpful because it can produce high resolution images at large magnification levels. One important geometric attribute that has a significant influence on battery cycling performance is the particle size of active electrode material. In comparing the performance of three LiCoO₂ powders fabricated by different processing techniques, Choi [51] used SEM analysis to characterize the ranges in particle sizes produced by each technique. These powders were used as active cathode material in CR2032 coin cells combined with lithium metal anodes. Charge/discharge cycling showed that

smaller particle sizes increase cycle performance due to increased cathode surface area available for lithium intercalation. Smaller particle sizes also performed better in high temperature environments due to improved electrode flexibility. However, reducing particle size compromised the initial discharge capacity of the tested cells.

Dendrite growth was investigated by Orsin [52] using quasi in-situ SEM observations on batteries with LiMn_2O_4 cathodes and three different anodes. The anode materials used were lithium metal, copper, and graphite, which were characterized as lithium batteries, copper cells, and lithium-ion batteries, respectively. Orsin's [52] experiment captured dendrite growth via SEM without exposing the cells to the outside environment. This enabled the author to reconstruct and cycle the batteries after each subsequent observation. In order to do this, the batteries were sealed in polymer laminates that could be easily cut open and resealed during SEM investigations. A portable air lock vacuum chamber was used to transfer the cells between the disassembly and SEM locations, and the cells were cooled before being placed into the SEM to prevent electrolyte evaporation. Using this method, Orsin [52] was able to document lithium dendrite growth on the lithium and copper electrode with respect to the applied discharge current. The authors were able to note the deterioration of the anode/separator interface due to dendrite growth, which caused a drastic decrease in cell performance. The authors also observed that the graphite anode was able to mitigate lithium dendrite growth, even at discharge rates as high as 2C.

Electrolyte

The electrolyte is a large contributor to capacity fade, resistance increase, and over all cell performance. Aside from monitoring the electrolytic resistance using EIS as described earlier, a battery must be disassembled in order to analyze electrolyte degradation. The effects of electrolyte solvent co-insertion into graphite anodes were investigated by Jeong [53]. Cells were constructed with graphite anodes, LiClO_4 cathodes, and three different ethylene carbonate (EC)

based solvents. The cells were disassembled and atomic force microscopy (AFM) was performed on graphite anodes before and after a charge/discharge cycle for each of the three solvents. AFM micrographs showed particle precipitates that had adhered to the graphite substrates after the first cycle. AFM scans were continued over the surface of each electrode until the precipitates were scrapped off by the AFM tip. After precipitates were removed, AFM micrographs revealed several pockets or “blisters” on the surface of each electrode, indicating solvent insertion into the inner layers of graphite upon cycling. Solvent insertion was shown to influence the composition of the SEI layer and it is also a known mechanism of electrode degradation.

Gas evolution due to electrolyte solvent break-down was studied by Kong [54]. Three different lithium-ion battery chemistries (LiCoO_2 , LiMn_2O_4 , LiFePO_4) with electrolytes containing LiPF_6 dissolved in a mixture of ethylene carbonate and diethyl carbonate (DEC) were constructed. These batteries were specifically designed for testing as the entire cell was sealed in a plastic membrane and a small hole was drilled in the top of the external casing. After cycling, a syringe was placed through the hole to pierce the membrane and collect gases generated during cycling. The collected gas was fed through a gas chromatograph and a mass spectrometer. It was found that during normal charging conditions the gaseous atmosphere is influenced by the reduction of DEC and a radical on the anode surface, as well as the reduction of EC, whereas during overcharging abuse conditions, the atmosphere is also influenced by the oxidation ability of the cathode material.

Electrolyte breakdown is often induced by heat generation within the cell; thus, thermal stability is a key issue for battery performance. Wang [55] investigated the thermal stability of an electrolyte composed of LiPF_6 dissolved in EC and DEC by cycling coin cells. The cells were then disassembled in an argon-filled glove box and then sealed in an inert pressure vessel where they were analyzed during heating from 0 to 300°C. It was found that the exothermic reductions

of EC and DEC occur at 164°C and 198°C, respectively. These values were realized by measuring the amount of heat flow that occurred with respect to the vessel temperature. However, when the two solvents are combined there is only a slight increase of heat flow at 192°C, indicating that the mixture is more stable than the two solvents by themselves. When the lithium salt is added to the mixtures, exothermic processes begin at lower temperatures for the DEC and EC/DEC mixture but begin at a higher onset temperature for the EC solvent by itself.

The techniques mentioned above require direct observation of internal battery components which is achieved only through a deliberate and systematic disassembly process. During disassembly there is a risk of introducing new defects or external contaminants which may potentially influence failure analysis results. Therefore, care must be taken to preserve the original state of the cell so that the failure mechanisms that progress during operation can be observed. The progression of these mechanisms is illustrated in Fig. 10. The remainder of this section outlines the considerations that should be taken when disassembling a battery in order to produce test results that are indicative of the true operating state of the battery.

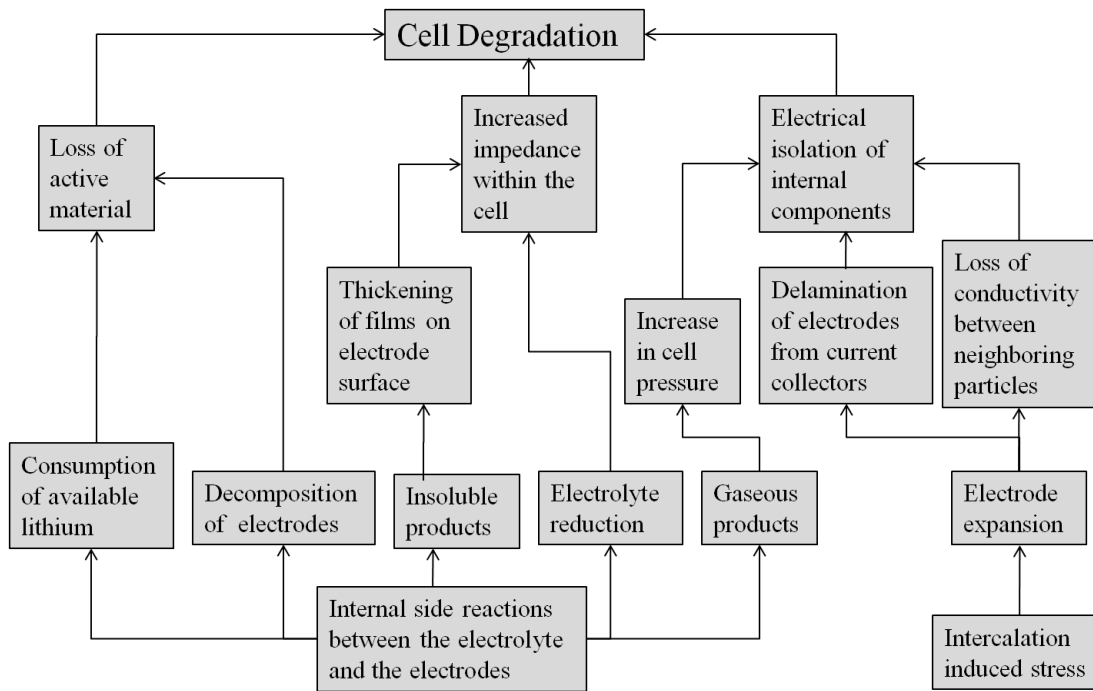


Fig. 10 Progression of mechanisms that lead to cell degradation.

Safety

Before a battery is disassembled, precautions must be taken to ensure the safety of any handlers during the disassembly process. First, all materials in the battery should be known before the exterior case is opened. Most commercial secondary lithium-ion batteries are composed of a LiCoO₂, LiFePO₄, or LiMn₂O₄ cathode, an electrolyte containing LiPF₆ dissolved in organic solvents, and a graphite anode. Manufacturer datasheets or technical guides should be consulted to obtain this information. If this information is not readily available, the analyst should contact the battery manufacturer to obtain this information.

Electrodes are often fabricated in powder form (held together by a binder material), so there is the potential of dust inhalation during disassembly. Dust inhalation can lead to upper respiratory irritation, lassitude, and generalized malaise, especially from metal oxides. In the cathode, health

concerns are mainly associated with the toxicity of the transition metal. This is one reason manufacturing efforts have attempted to veer away from LiCoO₂ cathodes. The Occupational Safety and Health Administration (OSHA) placed an exposure limit on Co at 0.1 mg/m³ due to its classification as a liver and kidney toxin, and it is considered a possible carcinogen [56]. With long-term exposure, manganese oxide has been known to act as a neurotoxin with Parkinson's syndrome-like effects [57]. OSHA's permissible exposure limit to manganese dust is 5 mg/m³. Less toxic cathodes include lithium iron phosphate and metal sulfides such as copper sulfide (CuS) and titanium disulfide (TiS₂); however, such materials may compromise battery performance due to their higher electrical resistance properties.

The electrolyte is the most volatile part of a battery and may emit vapors during disassembly. Organic solvents used in many commercial electrolytes include ethylene carbonate (EC) and diethyl carbonate (DEC). These are clear liquids that often have sweet odors. Acute exposure may cause lung, skin, or eye irritation. Lethal doses in rats have been reported at around 10,000 mg/kg for EC and 15,000 mg/kg for DEC, which are relatively high amounts and are comparable to the lethal dose of ethyl alcohol [58]. During disassembly, heat generation can lead to exothermic breakdown of the organic solvents, posing a possible fire hazard. Also, at increased temperatures, solvents will undergo decomposition reactions with other battery materials that could produce pentafluoride compounds, carbon monoxide, carbon dioxide, and hydrocarbons [56]. These products can form during battery usage and may be latent within the cell's case. Exposure to these fumes during disassembly should be avoided as they may be harmful to the eyes and throat and may cause skin irritation.

Lithium salts dissolved in organic solvents provide the mechanism for ion transport. After disassembly these salts can appear as white or off-white powders that appear after solvent evaporation. Lithium hexafluorophosphate (LiPF₆) is the most common salt used in lithium-ion

batteries, but other salts include lithium perchlorate (LiClO_4) and lithium trifluoromethanesulfonate (LiCF_3SO_3). Acute exposure to these salts can cause complications in the upper respiratory tract, and kidneys. Delayed effects after exposure have been reported and include nausea, thirst, drowsiness, tremors, and in severe cases coma or death from cardiac or pulmonary complications [59]. Even with the potential harmful effects of lithium salts, many have not been assigned permissible exposure limits at the time of this publication. Reaction of LiPF_6 with water will produce hydrofluoric acid, which is extremely corrosive to the eyes, skin, and mucous membranes. In cases where disassembly is conducted without moisture control, exposure to LiPF_6 should be limited to less than 3 parts per million (ppm) [60] through the use of a glove box or fume hood.

Many electrolyte additives have been proposed to improve battery performance by aiding in the formation of stable solid electrolyte layers, subduing gas generation, and reducing fire hazards [61]. These compounds usually make up no more than 5% of the electrolyte by volume but should still be considered when evaluating the safety hazards of disassembly. Acrylonitrile, for example, has been proposed as a preliminary film-forming additive to reduce solvent co-intercalation and suppress gas generation during the SEI formation period [62]. This additive can cause severe health effects with skin contact, inhalation, or digestion, and it is considered a possible human carcinogen. OSHA has placed an exposure limit of 10 ppm on the compound [63]. Boron-based anion receptors such as tris(pentafluorophenyl) borane (TPFPB) have also been proposed as electrolyte additives [64]. Their interactions with anions of lithium salts such as LiF allow for better solubility in carbonate solvents. This reduces the amount of precipitates that adhere to electrode surfaces and hence slow the increase of internal resistance. TPFPB has been reported to be an irritant to the eyes, digestive tract, and respiratory tract and may cause further irritation if it is absorbed through the skin.

There has been a considerable amount of research into alternate materials for battery electrodes. LiNiO₂ is sometimes used as a cathode material because of its high capacity to store lithium [65]. However, it suffers from poor thermal stability in its delithiated state due to the relative ease of reducing Ni³⁺ [66]. When LiNiO₂ batteries are disassembled, extra care should be taken to avoid external sources of heat and short circuits between the anode and the cathode which could cause LiNiO₂ to undergo an exothermic reaction at around 200°C [67]. Metallic lithium [68,69] has been widely researched as an anode material for its high negative electrode potential and high specific capacity. However, metallic lithium reacts aggressively with water, releasing flammable hydrogen gas and posing a serious explosion or fire threat during disassembly. Lithium anodes are also notorious for promoting dendrite formation and growth. Dendrites can puncture the polymer separator and cause an internal short circuit between the electrodes. These inherent safety concerns have prevented metallic lithium from ever reaching commercialization. Yet lithium foil is often used in R&D settings, especially as a counter electrode during impedance tests. In situations where reactive materials are used, a dry inert environment should be considered before a battery is opened. Material safety data sheets should be referred to on a case-by-case basis when disassembling batteries with unfamiliar materials.

Batteries undergo a high degree of scrutiny before they reach the marketplace. This examination, has driven many safety innovations over the years. Safety vents are now added to the external housing of batteries to release internal pressure build up from gas generation, and thermal fuses can be placed in battery packs to create an open circuit if a preset upper current threshold is reached. Microporous separators have an unintentional safety property known as separator shutdown that is displayed during overheating. As temperature increases and the polymer separator softens, the micropores begin to close, causing the complete blockage of ion transport. If there is a sufficient window available between the time that the separator cuts-off ion transport and the time that it melts completely, the battery can dissipate heat before reaching a thermal run-

away condition [70,71]. Other safety techniques include redox shuttles, which are added to the electrolyte. During overcharging, redox shuttles oxidize at the cathode while being reduced at the anode, which effectively transfers charge back to the cathode to prevent damage to the electrodes. These safety measures and the utilization of stable materials have greatly reduced the risk of fire and explosion even under abuse conditions. Eom [72] performed a nail penetration test on a 1000 mAh pouched lithium-ion cell. In this test a steel nail was driven through a fully charged cell perpendicular to the electrode plates. The author reported a temperature increase to 82°C, but no explosion, fire, or smoke were observed. Furthermore, many standards for battery manufacturing require safe performance under harsh physical abuse. Underwriters Laboratories' UL 2054 standards on household and commercial batteries require that a battery not explode or catch fire during a crush test with an applied force of 3000 pounds. However, there are still incidents reported of consumer batteries that have posed fire hazards. In 2009, Hewlett-Packard Co. issued a recall on 70,000 battery packs for their Compaq notebook computers due to two reports of battery overheating that led to rupture and flames [73].

All disassemblies should be conducted with proper protective gear, including chemical resistant gloves and chemical goggles. To avoid respiratory problems and minimize exposure to chemical vapors, a battery should be opened in a well-ventilated space such as a fume hood with a minimum draw of 60 to 100 FPM [74]. In cases where a fume hood is not available, an approved ventilator for protection against inorganic dust should be worn [56]. For more volatile battery chemistries, disassembly in a dry glove box with an inert argon environment should be considered.

If the handler notices excessive heat generation during the disassembly process, the battery should be placed in a well-ventilated area at a safe distance and given a sufficient time for internal reactions to expire before the battery is handled again. Heat generation is primarily a

concern when internal exothermic reactions caused by a short circuit or by high voltage potentials generate more heat than the battery is capable of dissipating. This can cause an uncharacteristic rise in the internal temperature, which then leads to thermal runaway. As a precaution in case of a fire, CO₂ or a dry chemical extinguisher should be on hand [56]. Water should never be used on lithium-ion batteries.

Choosing a Disassembly Environment

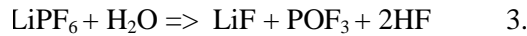
Before disassembling a battery, the atmospheric conditions where the cell will be opened must be determined. Choosing the correct disassembly environment is necessary not only to ensure safety but to preserve the failed state of the cell. This allows post disassembly test results to better reflect battery materials in their in-use state, which is generally of interest in research.

An environment containing an inert gas with oxygen and water contents maintained below 5 ppm is suitable for most battery disassemblies, but there are some cases where partial or total air exposure would not significantly influence post-disassembly test results. Considering that the cost of maintaining a glove box increases for each condition that must be controlled, the optimal disassembly environment can allow for certain cost-saving trade-offs.

When choosing the disassembly environment, there are two major considerations that must be taken into account. First, as mentioned in the safety section, the battery chemistry must be considered. Investigators should postulate how the chemistry of the battery has evolved with respect to usage, and how it will evolve further upon exposure to air, moisture, and heat. These chemical changes are evaluated to ensure the safety of the handler and the preservation of the test sample. The second consideration involves the nature of the tests being conducted. Certain investigations require a higher degree of chemical consistency between the operational state of

materials and the disassembled state of materials. The end goal of the test will determine the degree to which cell preservation must be maintained.

As described previously in the safety section, commercial lithium-ion batteries must pass stringent safety requirements and thus their materials cannot be prone to explosion or fire hazards. It has been shown [75] that lithium intercalation compounds with chemical potentials less than -3.5eV can sufficiently store lithium without it reacting to outside air or moisture. These compounds are ideal for battery fabrication because they are stable in air. Furthermore, the graphite anode and lithium metal oxide cathode contain no (or very little, as will be discussed later) metallic lithium, which does react exothermically with water moisture in air. Thus it is generally safe to assume that the electrode materials used in commercial batteries will not pose a thermal-related safety hazard in air at room temperature. During disassembly, the stability of the electrolyte is the primary concern especially in moist environments [76]. Exposure of lithium salts, namely LiPF₆, to water will lead to the exothermic reaction:



Thus, disassemblies should always be conducted in dry environments. For small single cell batteries, such as button cells, the content of lithium salt is small enough that no immediate fire or explosive hazards are present during careful disassembly in a typical indoor environment. However, there are still hazards due to toxic chemical exposure, such as hydrofluoric acid identified in the previously stated reaction. At a bare minimum, for small commercial lithium-ion batteries that were subjected to non-abusive cycling conditions, disassembly can be safely performed in a fume hood with a draw of 60–100 feet per minute (FPM) to prevent inhalation of toxic gasses or dust.

Disassemblies in a fume hood do not ensure chemical consistency between in-use materials and the materials after disassembly, so this environment should only be used when conducting “top level” investigations. Top level refers to investigations where the user is interested in basic internal properties, such as electrode dimensions, particle size/distribution, mechanical integrity, or screening for manufacturing defects such as internal shorts. These types of investigations require a top-level structural consistency between the in-use active materials and the materials after they have been removed from their external case. For top-level investigations, the disassembly methodology is much more important than the disassembly environment. If the cell is not deconstructed correctly, internal shorts or other user-induced mechanical damage may compromise failure analysis findings.

Tests aimed at sensitive compositional analysis of the cathode, electrolyte characterization, and surface morphology, as well as tests that require further electrochemical analysis on disassembled electrodes (reconstruction method), should be conducted in a dry, inert environment, such as an argon-filled glove box. As discussed earlier, the electrolyte is very sensitive to water moisture present in air [76]. The reaction between water and LiPF₆ can introduce heat and precipitates onto the surface of the battery electrodes. Also, the production of hydrofluoric acid from this reaction can cause cathode degradation [77]. Because the electrolyte makes up more than 10% of the battery’s mass [78], the damage and contaminants brought on by electrolyte decomposition can have substantial adverse effects on post-disassembly test results.

Huggins [79] proposed another interaction between water moisture with lithium ion battery electrodes. He suggested that materials with potentials above the stability range of water, such as LiCoO₂, LiNiO₂ and LiMn₂O₄, can absorb electrons and protons from moisture in the air. These materials oxidize water, releasing molecular oxygen, and in turn are reduced by the insertion of hydrogen (protons) and charge-balancing electrons into their crystal lattice structure. These

protons and electrons occupy sites that would otherwise be available for lithium insertion. This reduces the material's overall potential and lithium storage capacity.

If there is a chance that metallic lithium will be present during disassembly, then both moisture and oxygen should be restricted from entering the disassembly environment. Even though it is generally accepted that lithium in its metallic state does not contribute to a battery's faradic process, there are situations in which metallic lithium could exist on or within the battery electrodes. C. Smart [80] has suggested the possibility of lithium plating on carbonaceous anodes during low-temperature charging conditions. Reduced temperature can hinder ion diffusion into the graphite electrode, causing lithium to build up on the electrode surface. This build up can lead to dendrite formation, which may cause internal short circuits during operation but could also cause problems during disassembly due to lithium's reactivity in air. This process is thought to be reversible upon discharge, and, therefore, is more relevant in cells disassembled in a charged state.

Furthermore, there is evidence that suggests lithium in its metallic form may always exist around the edges of intercalated graphite regardless of the operational temperature. Hightower [81] investigated LiC₆ and metallic Li and found that both exhibited similar oxidation tendencies during examination under transmission electron microscopy. The author also demonstrated that the electron energy-loss spectra of LiC₆ edge sites more closely resembled metallic Li than Li⁺.

Small amounts of metallic Li present in graphite anodes will have the tendency to rapidly form Li₂O when exposed to oxygen. This reaction becomes problematic from an analysis standpoint when investigating phenomena such as the solid electrolyte interface (SEI). A previous investigation by Golodnitsky [50] found an SEI layer to be partially composed of Li₂O. However, the authors do not provide enough details about the disassembly process or specify a

means of controlling oxygen exposure. Thus, their results could have been skewed by oxygen contamination. It is possible that oxygen was present during the assembly process or had been generated during cycling due to cathode reduction. However, the contribution of the oxygen introduced during assembly, usage, and disassembly cannot be differentiated unless the environment is properly controlled.

As outlined above, water can have hazardous and property-changing effects on many of the battery components, while oxygen can affect residual metallic lithium contained in the anode. Thus, situations where it is acceptable to conduct disassembly in a fume hood, in a glove box with an inert gas and moisture regulation, or in a glove box with an inert gas, moisture regulation, and oxygen regulation, are given in Fig. 11.

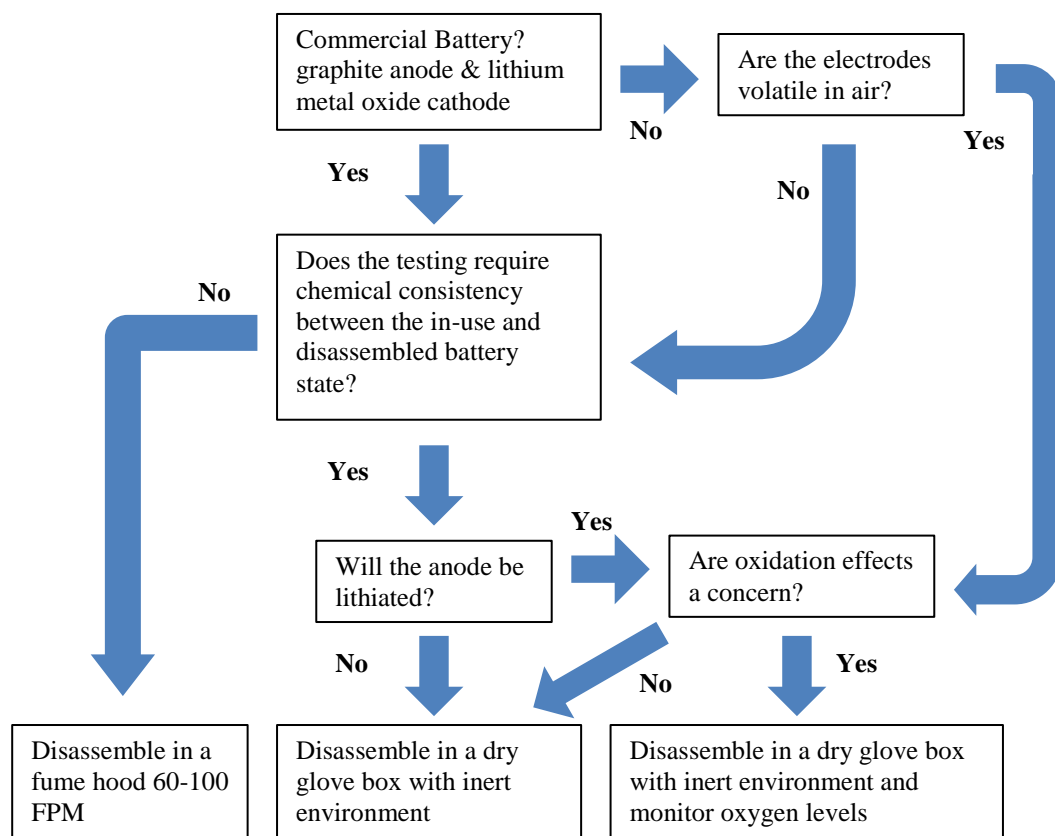


Fig. 11 Flow chart to determine the disassembly environment

Disassembly Method

The following disassembly process was demonstrated on a single cell prismatic lithium-ion battery. This method may vary slightly depending on each battery's particular form factor; however, the following steps are generally applicable to most cylindrical and pouched lithium-ion cells. This disassembly was performed in an argon-filled glove box with moisture content kept below 5 ppm as indicated by the glove box sensor. This simulates testing that requires a "dry glove box with inert environment" as prescribed by the flowchart in Fig. 11.

For this disassembly, examination of the lithiated anode was not a concern. In order to place the cell at a lower potential energy state and minimize the amount of charge in the event of an accidental short circuit, the battery was discharged to 100% depth of discharge, or 2.7V, as per the manufacturer's specified cut-off voltage. This discharge state effectively removed residual lithium from the graphite anode to ease concerns of electrode instability.

If the cell is part of a battery pack, it should first be removed from the pack casing. Depending on the pack construction, the casing can be disassembled simply by removing the screws that hold the pack together, or it can be cut open carefully with a carbide-tipped saw. X-ray imaging should be used to avoid cutting into the individual cells held in the pack. The cells inside of a battery pack may be connected in parallel and/or in series and should be separated so that each individual cell is stripped down to its casing alone. Battery packs may contain complex control circuitry or a battery management system (BMS), which should also be removed. The disassembly process should avoid accidental shorting of the internal cells.

A single cell battery should be stripped down so that all that remains are the external case and the cell itself. This usually means removing the manufacturer's sticker label and the safety circuit, which is most often attached to the top of the cell soldered to the external leads. The external safety circuit can be removed by simply sliding a blade under the circuit housing and prying it up.

If necessary, X-ray images should be consulted when the safety circuit connection is not clearly visible under optical inspection. Wire cutters can be used to cut the connections between the leads and the external circuit, or the leads can be de-soldered. Often the entire outside case of the battery acts as the positive terminal, while the negative terminal protrudes from a tab at the top of the case. When cutting the connection between the leads and the safety circuit, caution must be taken not to create a short between the negative tab and the positive case.

At all times during cell disassembly, the most common cause of post-testing defects is the introduction of internal short circuits between the two electrodes. This causes rapid high-rate discharge, generating excessive heat and leading to electrolyte decomposition. To avoid accidental discharge, conductive tools should never come into contact with both terminals at the same time. Also, excessive force should not be applied on the casing. If the cell is fixed in a vice or if pliers are used during the removal of the safety circuit or the dismantling of the battery pack, care must be taken not to compress the cell past its original case width. Too much compressive force can cause a puncture in the separator and short the anode and the cathode.

After the battery has been reduced to its casing alone, X-ray images should be taken to identify the optimal location for a first incision. This will be the area where the electrodes are farthest away from the external case. This location should be large enough so that a cut can be made without causing any internal damage to the battery electrodes. Often this is at the top of the cell near the negative terminal, as shown in Fig. 12. When an ideal location is found, a reference mark should be made on the outside of the case, indicating the available cutting room.

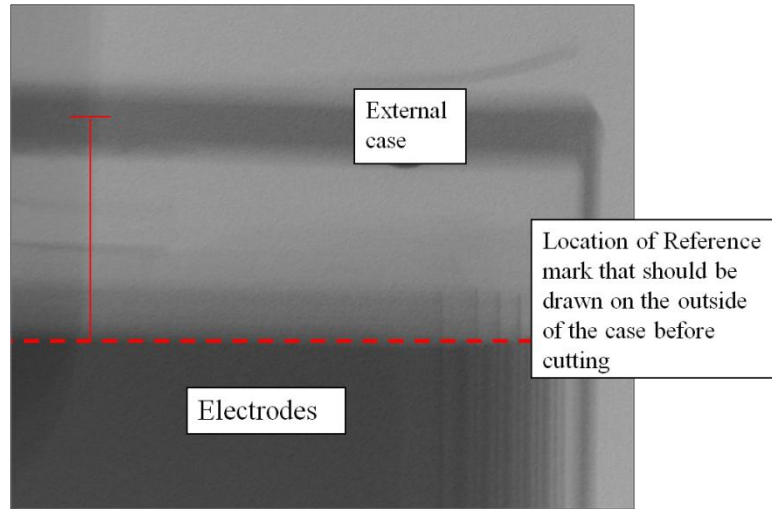


Fig. 12 X-ray investigation to find best spot for incision

A precision cutting device such as a Dremel® tool with a carbide-tipped saw should be used to make the first cut [Fig. 13 a]. This cut should be made along the reference mark designated during the X-ray inspection. The cut should be shallow and only penetrate one of the battery case's sides. It should extend across the entire width of the battery case.

After making the cut, pliers or wire cutters can be used to pry back the top of the battery case [Fig. 13 b]. The top should still be connected on one side of the case in order to open it like a lid. At this point, the lid can be gripped with the pliers and twisted so that the battery casing begins to peel away from the internal cell [Fig. 13 c]. This can be continued until a quarter of the case has been peeled off the cell. The cell should now be ready to be removed from the case. To do this, the cell should be gripped gently by a pair of tweezers and pulled from the case. Caution must be taken not to grip the cell too tightly, which could puncture the separator and cause contact between the anode and the cathode. If the cell is stuck, it should not be forced out. Instead, the casing should instead be peeled further until the cell can be easily removed. If the disassembly is successful, there should not be excessive heat or smoke generated.

The cell is disassembled in this way to minimize the amount of cutting into the battery case. This reduces the likelihood of cutting too far past the case and damaging the cell. Also, cutting into the metal case will create dust, which can contaminate the cell. In this situation it becomes difficult to correctly analyze the battery because failure sites caused during the battery's use may not be distinguished from failures caused by the battery's disassembly.

In the case of lithium polymer batteries, the battery case is not a rigid metal but a soft foil wrap. The soft foil is much easier to cut with readily available instruments such as a pair of scissors. In the case of cylindrical cells, the pry and twist method might not be applicable; In this situation, it could be better to use the method described by Aurbach [32].

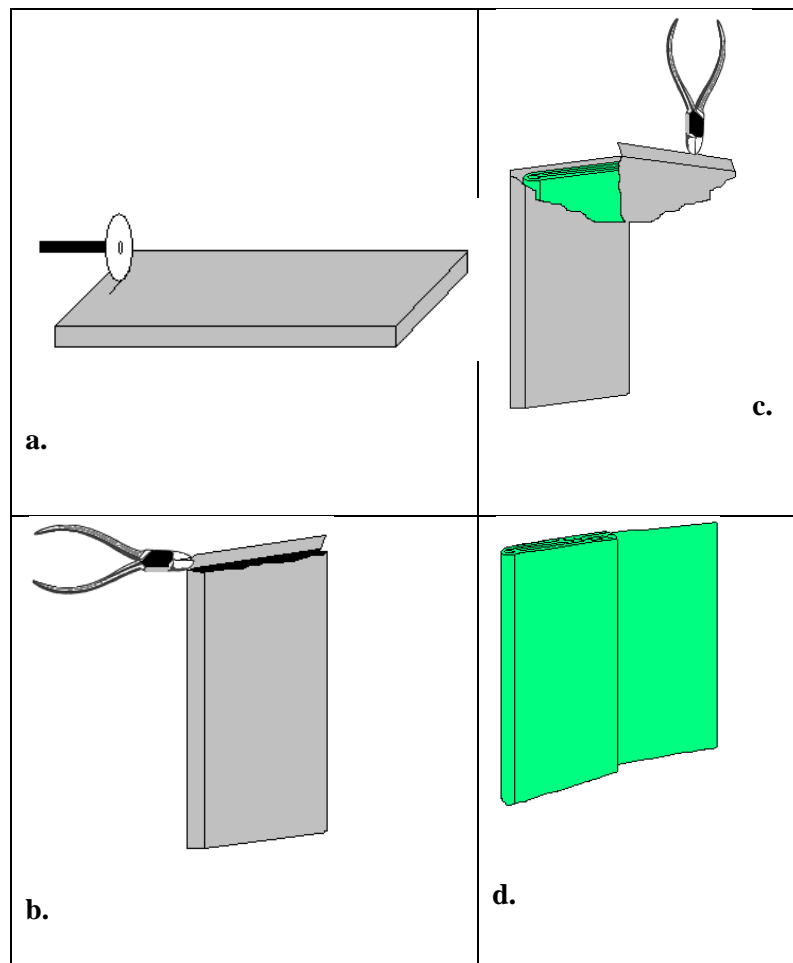


Fig. 13 a) The initial incision is made, avoiding internal active material; b) the top of the case is pried up so as to create a “lid”; c) the lid is twisted so that the case begins to peel away from the active material; d) the internal components are removed

Post-Disassembly Processing

When the cell has been removed from its case, it must be handled in a manner that is conducive to the analysis to which it will be subjected. If the purpose is to perform compositional analysis, the cell can be unrolled [Fig. 13 d] and each constituent part of the battery separated without focusing too much concern on the structural integrity of the electrodes. Aurbach and Wu [32,49] pulverized their electrodes in order to perform powder XRD. If the purpose is to investigate mechanical properties of the active material or to evaluate the electrode's construction, the cell should not be immediately unrolled. Cathode electrodes are relatively flexible, but graphite anodes can crack and flake during the unrolling process. If the electrodes are unrolled, observations should be taken from the flat portion of the electrode rather than the rounded edges, which sustain the most stress during the unrolling process. Another option that does not require unrolling is to perform cross-sectional analysis. This can be performed by mounting the cell in an epoxy resin similar to the methods used in semi-conductor analysis. After the sample has cured it can be grinded using abrasive paper to a selected depth where a cross-sectional region can be viewed Fig. 14. This must be done in a well-ventilated area due of the safety hazards associated with breathing in dust from the active material (see safety section).

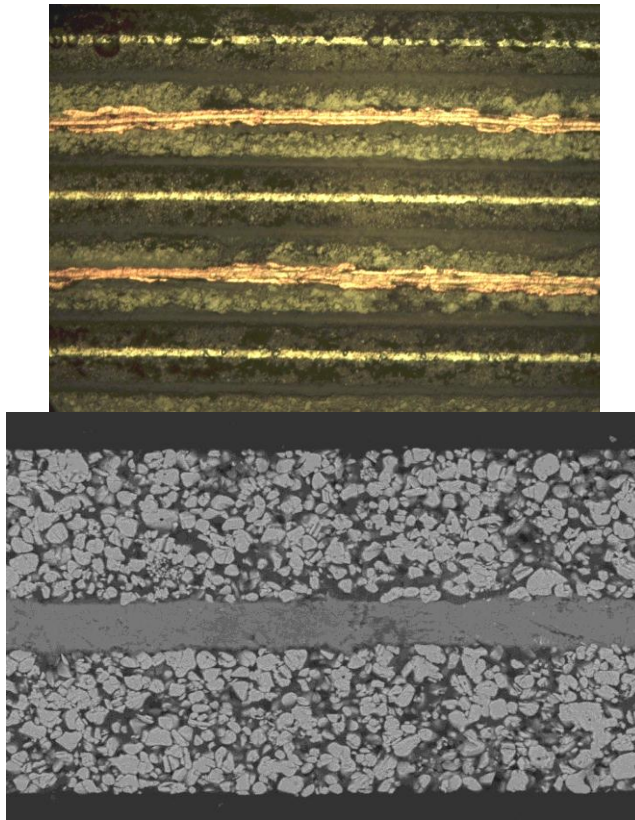


Fig. 14 Optical microscope image of stacked electrodes after cross-sectional analysis (top); SEM image of cathode taken after cross-sectional analysis (bottom).

In some cases, researchers have chosen to soak the disassembled electrodes in dimethyl carbonate (DMC) or another similar solvent [82] as a post-processing procedure to clean the electrodes before observation. In other cases, such as in Aurbach's [32] work, the electrodes were not soaked or dried before analysis. The practice of electrode cleaning has led to some disagreement within the battery literature, as noted by Orsini [52]. The general purpose of soaking is to remove residual electrolyte and heavy elements from the electrode surface; however, in doing so it is possible that some components of the SEI layer can be lost. The SEI layer is made up of the decomposed products of the electrolyte. Some of these products build up during cycling and, over long rest periods, gradually dissolve back into the electrolyte. This phenomenon is observed through the regeneration of a battery's maximum capacity during rest. The soluble products responsible for this phenomenon can be lost

during an electrode cleaning process, and only the SEI components responsible for irreversible capacity loss will remain.

If the electrodes are not cleaned, a given amount of electrolyte residue, mostly composed of a lithium salt, will be left on the surface of the electrodes after evaporation of the organic solvents. This residue, which was not an original contributor to the SEI layer, may be difficult to distinguish from surface films that formed during usage. Orsini [52] approached this problem by cooling down the sample during his in-situ SEM investigations. This reduced the vapor pressure of the electrolyte and prevented evaporation during scans in the vacuum chamber. In general, soaking may lead to an absence of particular SEI components, while not soaking may introduce new residue on the electrode surface. In either case, the effects of cleaning should be taken into account when determining the actual in-use composition of electrode surface films.

When transporting between the disassembly location and the testing site moisture and oxygen levels must also be controlled. Maintaining large-scale dry rooms and controlled environmental test labs is expensive and not always feasible. In such situations, battery materials can be transferred by enclosing the materials in a vacuum-sealed container before they are removed from the glove box. In Hightower's experiment, [81] which observed the effects of air on LiC₆, he immersed his samples in Flourinert® FC-43 while still in an Ar-filled glove box to provide an inert environment during transport. Once the samples were placed in the load lock of the transmission electron microscope, the Flourent® was allowed to evaporate. Thus, observations could be made on the very first effects of air on LiC₆.

When performing failure analysis on battery materials it is important to consider how the method and environment of disassembly will affect the final results. Due to the possible presents of metallic lithium and volatile nature of the electrolyte it is important to understand

how these components will react with air and water moisture upon removal from the hermetically sealed battery case. This must be approached from both a safety stand point as well as an analysis standpoint because typically the goal of failure analysis is to investigate the effects of usage on battery materials. By controlling the disassembly environment and using a deconstruction method that minimizes the damage to battery electrodes, the changes in cell chemistry due to the disassembly process can be negated and the true causes of internal cell degradation can be isolated.

3. Performance Testing

This study investigated the effects of different types of usage conditions and battery constructions on performance and reliability. These differences were then characterized through data analysis and failure analysis. Testing involved commercial Li-ion batteries subjected to a number of different charge/discharge profiles to identify the effects of simulated usage conditions on capacity fade.

Test specimen

Three lithium battery models used in portable electronic applications with a nominal voltage of 3.7 Volts were selected for testing. The naming convention for the batteries is provided in Table 2. The “A” batteries were lithium polymer batteries. CS2 and CX2 batteries were lithium ion batteries. The tested of batteries are typically used in high energy applications as opposed to high power applications which imply they were optimized to supply low currents for extended periods of time rather than large bursts of current (which is a design feature for applications such as electric vehicles). High power applications often use cathodes such as LiFePO₄ where high energy applications often utilize a LiCoO₂ cathode. Thus we would expect the batteries in this study to be composed of a LiCoO₂ cathode and a graphite anode.

Manufacturer	Manufacturer A	Manufacturer B	
Naming Convention	A_x	CS2_x	CX2_x

Table 2 Battery types used in this study where the "x" is a number that identifies a particular battery

In order to verify the battery construction, the internal configuration of each battery was inspected after removal of the safety circuit, x-ray and disassembly of the battery samples. Several layers of active material were removed and prepared for an environment scanning electron microscope (ESEM) inspection. The elemental composition of active materials was detected using energy dispersive spectroscopy (EDS) to identify the prominent elements contained within the active material.

A Batteries

The A batteries are classified as lithium polymer with a rated capacity of 0.9Ah and a nominal voltage of 3.7V. They utilize a stacked polymer (Figure 15) configuration in which the separator is folded over in an accordion fashion. The anode and cathode materials are stacked in alternating folds, with their respective current collectors acting as substrates. The negative and positive tabs act as the battery's terminals and extend down to each current collector, connecting the electrodes in series. The battery casing is composed of a soft foil that expands as internal pressure increases.

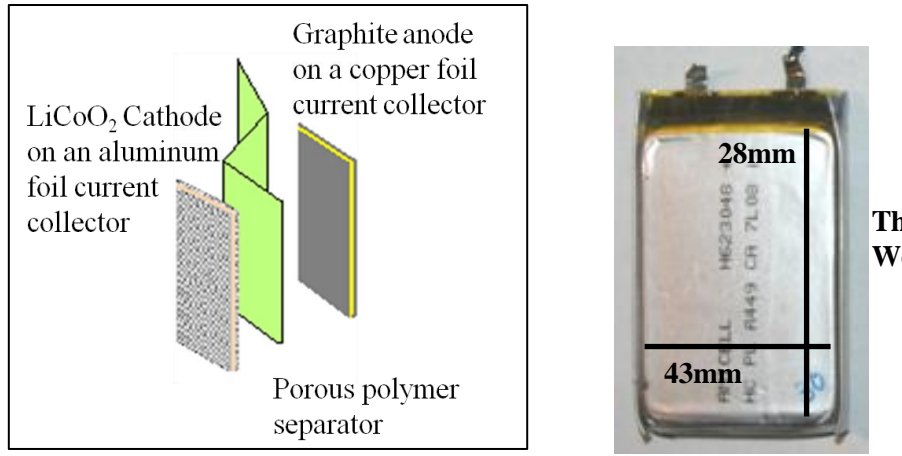


Figure 15 Construction of Battery from Manufacturer A

To further investigate the material properties of the battery specimen, a cross-section perpendicular to the plane of the electrode surface was performed and EDS mapping was used so that elements could be locally identified. The results are displayed in Figure 16 and show a copper anode current collector and an aluminum cathode current collector. This picture also shows that the anode and cathode material have been applied on both sides of the current collectors so that when each of these layers are stacked or rolled, they act as multiple thin cells on top of each other. Also the electrode geometry features were measured from the cross sections. It was found that the thickness of the anode was $73\mu\text{m}$ while the thickness of the cathode was $65\mu\text{m}$.

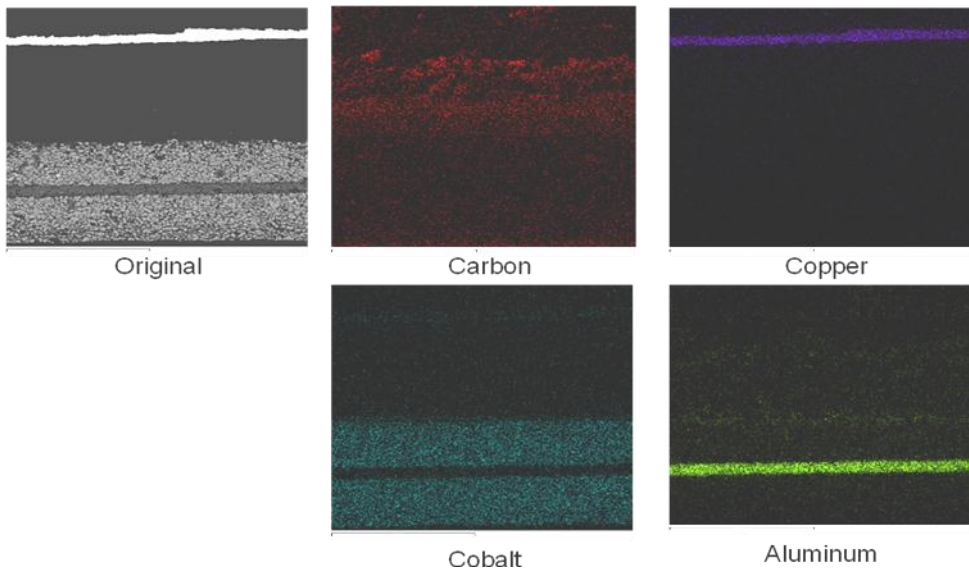


Figure 16 EDS mapping of battery cross section

From the EDS analysis, the cathode has cobalt on either side of the current collector and carbon is found on the anode current collector. This result supports the conclusion that the composition of the cathode is LiCoO_2 .

CS2 and CX2 Batteries

Both CS2 and CX2 batteries utilize a prismatic (Figure 17) configuration where the electrodes are deposited on long thin current collector sheets. Then the composite current collector/electrode and a separator are pressed together and wound up in a jelly roll-type arrangement. For the CS2 model, the electrodes are wound around the vertical axis of the battery while in the CX2 battery the electrodes are wound around the horizontal axis. In this configuration, the outside case is an extension of the cathode current collector and exhibits a positive polarity. The negative terminal is on the top side of the battery and it is formed by micro-welding a nickel tab to the negative current collector and then connecting the tab to the terminal. Both of these batteries utilize hard aluminum cases as opposed to the soft foil cases used by manufacturer the A batteries. The

CS2 model has a rated capacity of 1.1Ah and a nominal voltage of 3.7V and the CX2 model has a rated capacity of 1.35Ah and a nominal voltage of 3.7V.

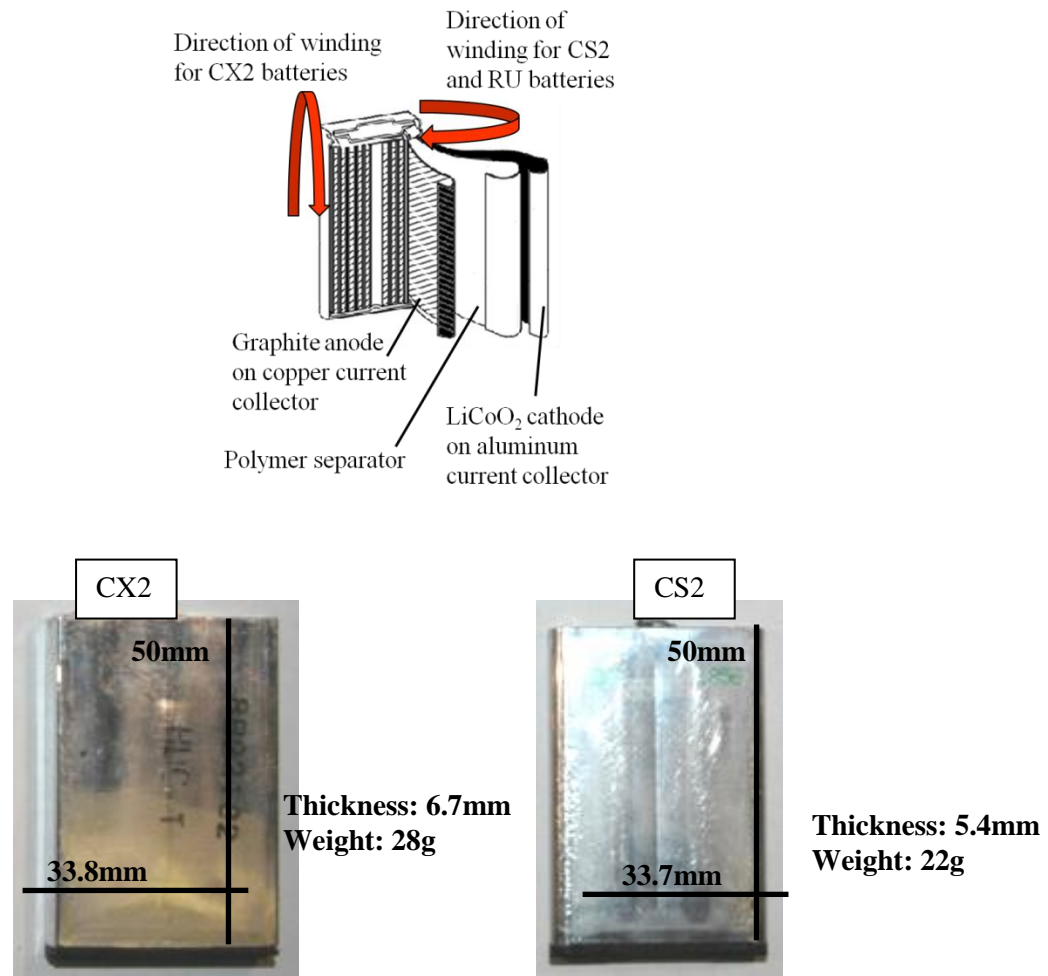


Figure 17 Construction of battery from Manufacturer B

EDS analysis was performed on both the CS2 and CX2 samples as well in order to confirm the basic elemental composition of the electrodes Figure 18.

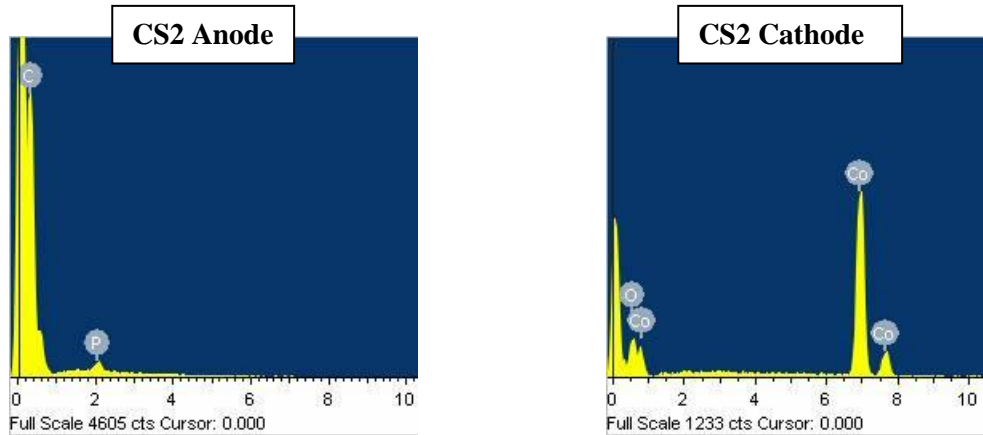


Figure 18 EDS on manufacturer B electrodes

While EDS confirmed that all three batteries have a similar chemistry that is consistent with typical commercial lithium ion batteries, it is likely that there are subtle differences between each type. These differences may include slightly different mixing ratios of the binder and active material or the organic solvents and lithium salts. Also, trace amounts of additives are often added to batteries to improve performance or reliability properties. However because these additives make up such a small percentage of the material in the battery it is hard to identify these substances using EDS, also the information regarding these slight chemical changes among batteries are often kept proprietary by battery manufacturers.

Cross sectional analysis showed that the anode thickness of the CX2 batteries 66 μm were slightly smaller than that of the CS2 battery 68 μm whereas the cathode thickness of both batteries were the same 63 μm Figure 19.

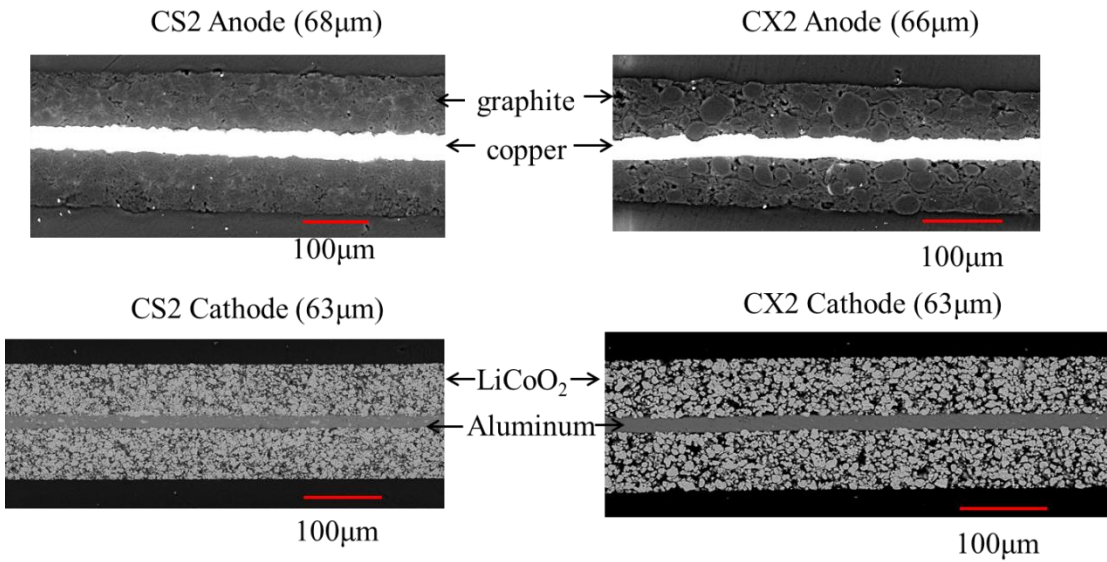


Figure 19 Cross section images of CS2 and CX2 electrodes

Test Types

All tests were performed on either one of two commercial battery testers. The first was a 4 independent channel, 400 watt Cadex C8000 battery analyzer; the second was a 16 independent channel Arbin BT2000 battery test system. Both testers were capable of running customizable charge and discharge profiles. Unless otherwise noted, all tests took place in ambient, lab temperature conditions which typically ranges between 20 and 25°C. For all the tests, current, voltage, and time data was taken periodically. For a selected number of tests temperature, internal resistance, and internal impedance measurements were also taken. The charging method for every test performed was the same, and followed the constant current/constant voltage charge protocol. This charging method applies a constant current of 0.5C until the voltage of the battery is measured to be 4.2V. After that, the power supply switches to a constant voltage charging mode where the battery voltage is held at 4.2V until the charging current drops to 50mA. At this time the charging profile was considered complete.

The discharge profiles were varied for each test condition and are described below. It should also be mentioned that due to the relatively small number of samples provided from manufacturer A, most of the structured test plans were based on samples from manufacturer B. The samples from manufacturer A were mainly used for comparison studies.

Cycle Life (Constant Current Discharge)

The cycle life tests at constant current discharge were performed considering the standards described in the UL 1642 and IEEE 1725 [83]. These suggested that batteries be cycled at room temperature to the specifications of the manufacturer such that their full capacity was utilized during cycling. A maximum charge cut-off voltage of 4.2 V and a minimum discharge cut-off voltage of 2.75 V was proposed by the manufacturer of the A batteries. A maximum charge cut-off voltage of 4.2V and a minimum discharge cut-off voltage of 2.7V was proposed by the manufacturer for both CS2 and CX2 batteries. As the name suggests, this test used a constant current to discharge the batteries from a fully charged state until they have reached their discharged state (as indicated by the discharge cut-off voltage). The test matrix for the CS2 and CX2 batteries is shown in Figure 20 where the discharge currents used were 0.5C and 1.0C. The Q_{max} was calculated after each discharge cycle and failure was considered to be the cycle number where Q_{max} fell below 80% of Q_{rated}

		Discharge Current Rate	
		0.5C	1.0C
Battery Type	CS2	Samples: 4 CS2_8 CS2_21 CS2_33 CS2_34	Samples: 4 CS2_35 CS2_36 CS2_37 CS2_38
	CX2	Samples: 4 CX2_31 CX2_33 CX2_35 CX2_16	Samples: 4 CX2_34 CX2_36 CX2_37 CX2_38

Figure 20 Cycle life test matrix

In order to compare the cycle life and discharge properties of these batteries the “A” batteries, four “A” batteries underwent charge/discharge cycling at a constant current discharge rate of 0.5C.

High Rate Discharge Test

The high rate discharge tests were identical to the constant current discharge test except discharges were performed at a constant current rate of 3C for the CX2 and CS2 batteries. Periodically the batteries were discharged at a rate of 0.5C in order to evaluate the rate capability. This metric describes a battery’s capacity at a high rate of discharge compared to its capacity at a low rate of discharge (0.5C in this case).

Pulsed Discharge Tests

The pulsed discharge test was performed on a CX2 battery. Rather than supplying a constant current discharge, this test used a current of 1C, 0.5C, and 0C each for 30 seconds. This profile was repeated until the battery reached its set cut-off voltage and then the standard charging protocol was performed over several charge/discharge cycles until the battery reached failure.

Continuous Charging

The continuous charging test assesses the ability of a battery to maintain its capacity while remaining charged for an extended period of time. “A” Batteries were first charged, then discharged, and then recharged at the manufacturer’s specifications in order to obtain a baseline capacity and assure that the cells were in proper working order. Upon reaching the end of charge voltage, the batteries were supplied a float charge so that they could remain just under their maximum potential, at a voltage of 4V, for 150 hours. After 150 hours, the

batteries were again subjected to a discharge/charge profile to obtain a second capacity measurement. After another 500 hours the procedure was repeated, and capacities and voltage discharge profiles were compared. IEEE 1725 requires that a battery undergoing continuous charging display no leakage, no visual evidence of leakage of electrolyte, no venting, no explosion, and no fire.

Shallow Charging

Shallow charging refers to a situation where a battery has been prematurely removed during charging and has not reached its maximum charge voltage. This condition has serious consequences for nickel-based batteries as they are susceptible to the memory where a pattern of partial charges leads to the batteries inability to undergo full discharges. Li-ion batteries do not display memory effects; however, there is some interest in how shallow charging might affect the reliability of a cell throughout its life cycle. In order to investigate shallow charging, one “A” battery was discharged to a 2.7V cutoff and then charged to a 3.7V maximum voltage as opposed to the manufacturer recommended 4.2V. The standard constant current constant voltage protocol was used except for the adjusted charge cut-off voltage limit. Because the cell was not required to reach its maximum potential, less ion transport was necessary, which greatly decreased the length of the cycling times. The cell was exposed to several hundred shallow charging cycles at .5C. After cycling under shallow charging conditions the maximum charge voltage was increased back to 4.2V and the cell were cycled using standard conditions until failure.

Shelf Life

Because of the degree of high free energy when a battery is in its charged state, there is a driving force that will cause some electrons to move through the electrolyte [84]. This migration of electrons while the battery’s external circuit is open is described as self-

discharge, and it defines the battery's shelf life. In order to investigate the rate of self-discharge, batteries were charged and discharged using the manufacturer-recommended conditions so that a baseline capacity reading could be taken. Once the batteries had been verified to be in proper working order, they were again supplied a current of 0.5C until they had reached a 100% state of charge. When the cells were in a fully charged state they were removed from the battery tester and placed in a thermal chamber set at room temperature (25°C). The open circuit voltage was measured periodically over time to monitor the rate of self discharge.

Random Cut-off Voltage Test

This can be viewed as a shallow discharge test. For this profile, a CS2 battery was always charged to its maximum charge voltage however during discharge, the current was cut-off before the battery was allowed to reach its minimum discharge cut-off voltage. However, rather than leaving the cut-off voltage fixed throughout the cycle life of the battery (as was the case in the shallow charging test) the cut-off voltage was randomly changed every 15 cycles to a value between 4.2V and 2.7V. This test was used to simulate the situation in which a user decides to re-charge a battery before it has been completely discharged.

The cumulative results of these tests provide insight into the response of battery reliability under various types of usage profiles. Based on these results, further testing (with more consideration placed on statistical significant) can be performed that highlight the test scenarios which showed the greatest influence on battery reliability.

4. Results and Discussion

Test Results

Cycle Life (Constant Current Discharge)

Figure 21 shows a typical charge/discharge current and voltage profile for the constant current discharge test. As described, the profile can be divided into three sections, a constant current charge, a constant voltage charge, and a constant current discharge. The beginning and end of discharge were determined by the cut-off voltages mentioned in the test type section.

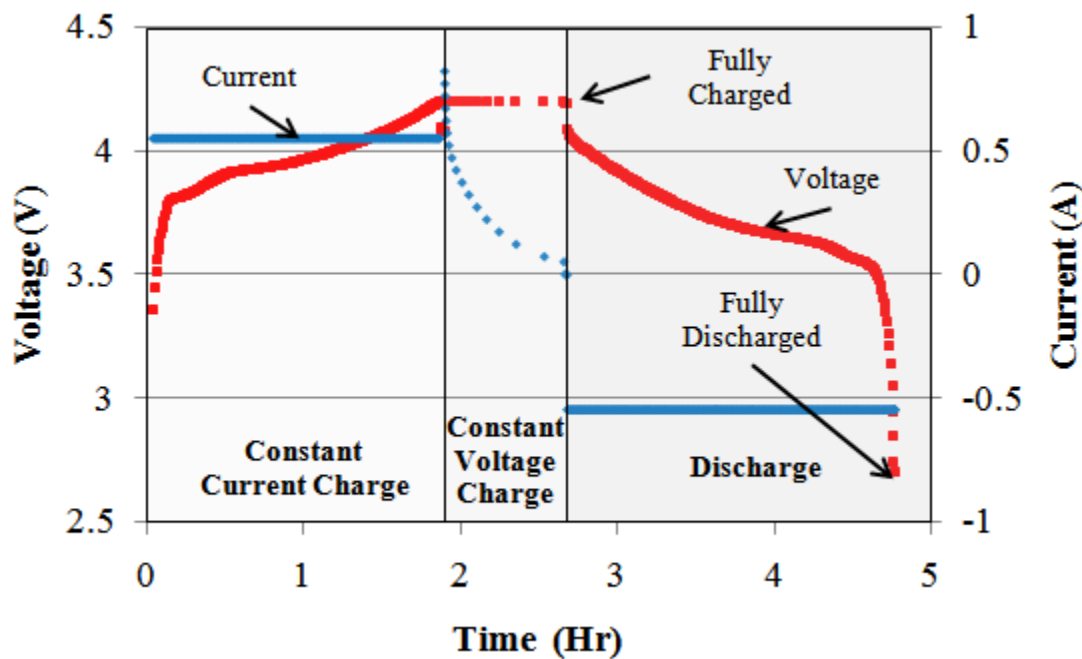


Figure 21 Charge/discharge profile for constant current discharge test

By cycling the test samples from a fully charged state to a fully discharged state, the Q_{max} was able to be directly calculated for each discharge cycle by integrating the current by time. Q_{max} was the feature of interest in this study and the failure criteria was set as when the Q_{max} of the battery degraded to 80% of the rated capacity. A large amount of information can

be deduced by analyzing the capacity fade curve. When a lithium ion battery is cycled under constant discharge and environmental conditions (hence stresses from the environment and usage profile are consistent from cycle to cycle) the fundamental trend in capacity fade can be divided into three parts as shown in Figure 22.

For the first 50 cycles, the rate of capacity decrease is slightly higher than what is observed over the next several hundred cycles. This first stage of capacity loss can be considered to be the formation period. During this time lithium reacts with organic solvents in the electrolyte at a close vicinity of the electrodes in order to form the SEI layer. This consumes lithium reducing the number of charge carriers available in the battery. This stage lasts until the electrodes have been sufficiently coded in surface films such that a passivation layer is formed over the electrodes preventing further reactions. At this point, the capacity degradation progresses in a linear fashion over the next 500 cycles. This is the second stage of capacity loss and most of the operational life will fall within this stage. During this period, battery capacity can be easily predicted due to its linear relationship with time allowing BMS to make accurate SOC and SOH predictions. The mechanism of capacity fade during this stage is likely the slow thickening of the SEI layer and increased internal resistance due to the constant expansion and contraction of the electrodes as described in the degradation mechanisms section. In the last 300 cycles shown in Figure 22 the rate of capacity fade begins to increase exponentially as the battery moves into the third stage of capacity loss. It is good to define a failure threshold before this knee in the capacity fade curve occurs because predicting the SOH and SOC of the battery becomes a much harder non-linear problem. Also the amount of operational time that the battery can provide the host system decreases sharply with each additional cycle. During the third stage of capacity loss, it is likely that an onset of many mechanisms occur. Besides increased thickness in the SEI layer and reduced cycleable lithium, gas evolution will occur due to the breakdown of the

electrolyte solvents as evident though the “ballooning” of the cell outer case. This can increase internal cell pressure causing the electrodes to crack and flake as well as increase the resistance of the electrolyte. The combined effect of this chain reaction of mechanisms leads to the exponential decrease in the battery’s capacity.

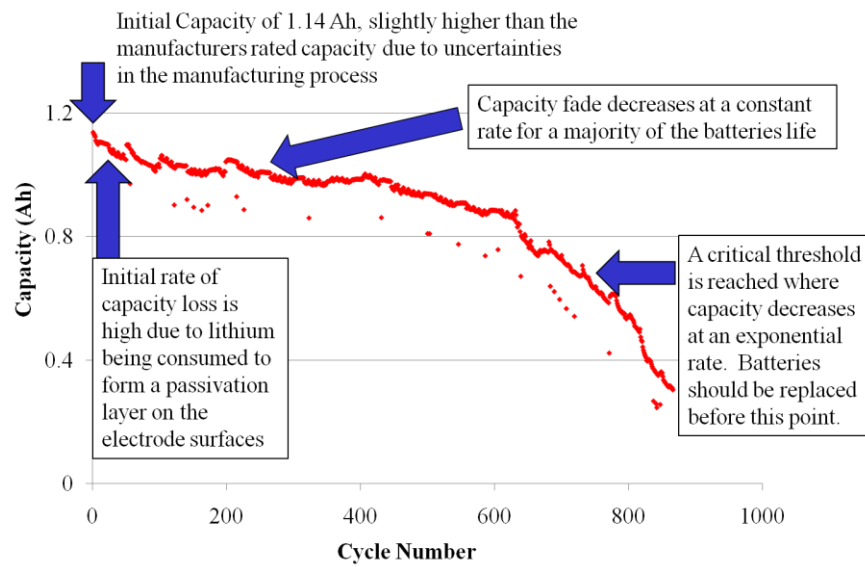


Figure 22 Analysis of capacity fade curve for a CS2 battery

An interesting phenomenon this data are the increases in capacity that occur every 50 cycles. This test was programmed to run for 50 consecutive cycles and then stop so that data could be collected and routine maintenance performed. The increase in capacity during these rest periods is attributed to soluble precipitates that build up on the surface of the electrodes during cycling and during rest they are allowed to dissolve back into the electrolyte. When this happens, any lithium contained within these precipitates returns back to the electrochemical process effectively increasing the capacity. This indicates that the layers on the electrode surface are composed of soluble and insoluble parts, where the insoluble parts result in irreversible capacity loss while the soluble parts contribute to recoverable capacity

loss. By plotting the amount of capacity recovery vs. the rest time a logarithmic trend was found and is shown in Figure 23.

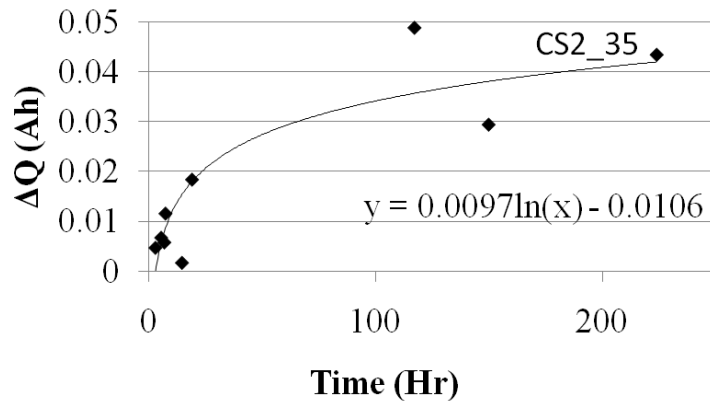


Figure 23 capacity recovery vs. rest time

The time to failure results of the 1C and 0.5C constant current discharge test for the CS2 and CX2 batteries are shown in Figure 24.

		Discharge Current Rate	
		0.5C	1.0C
Battery Type	CS2	Samples: 4 Cycles to failure (CTF)	Samples: 4 CTF
	CX2	CS2_8 471 CS2_21 730 CS2_33 537 CS2_34 515	CS2_35 608 CS2_36 480 CS2_37 601 CS2_38 661
	CS2	Samples: 4 CTF	Samples: 4 CTF
	CX2	CX2_31 1336 CX2_33 764 CX2_35 803 CX2_16 1321	CX2_34 669 CX2_36 741 CX2_37 747 CX2_38 724

Figure 24 Test matrix displaying the cycles to failure for each sample

To analyze the significance of these results, the time to failure data was fit to a Weibull distribution and plotted in Probability graphs. Figure 25 contains data for the CS2 batteries and Figure 26 contains data for the CX2 batteries. By viewing the overlap of the confidence intervals for the 0.5 and 1C data sets of the CS2 batteries in Figure 25 it is clear that there is no statistical difference in time to failure for the two tested discharge levels. This suggests that discharging this battery type at currents between 0.5C and 1C has a negligible effect on cycle life. For CS2 batteries a 1C discharge rate corresponds to a current of 1.1A. This current appears not to have accelerated side reactions within the battery suggesting that any heat generated by this discharge current was efficiently dissipated by the battery. However, Figure 26 shows that a clear difference in cycle life between the two discharge rates for the CX2 batteries can be observed. Because the CX2 battery had a higher rated capacity, the 1C discharge rate corresponds to a discharge current of 1.35A. The 1C current may have generated enough heat to cause reactions at the electrolyte/electrode interface to occur at a faster rate compared to the 0.5C level discharge.

Figure 27 compares the cycle life of CS2 and CX2 for both discharge rates. Here it is seen that even though the CX2 cycle life was more sensitive to a higher discharge rate, the CX2 batteries have longer life cycle characteristics than the CS2 batteries for both discharge conditions.

Figure 28 and Figure 29 show the actual discharge capacities for all the CS2 and CX2 batteries tested in the cycle life test. In these figures the blue horizontal line shows the rated capacity for each battery and the green line shows the failure threshold. Here the distribution of the beginning of life capacities around the rated capacity along the y-axis of the can be seen. Also the distribution of failure times along the x-axis can be noted. These differences can be mainly attributed to uncertainties in the manufacturing process and storage time that lead to variations in performance and reliability between each battery.

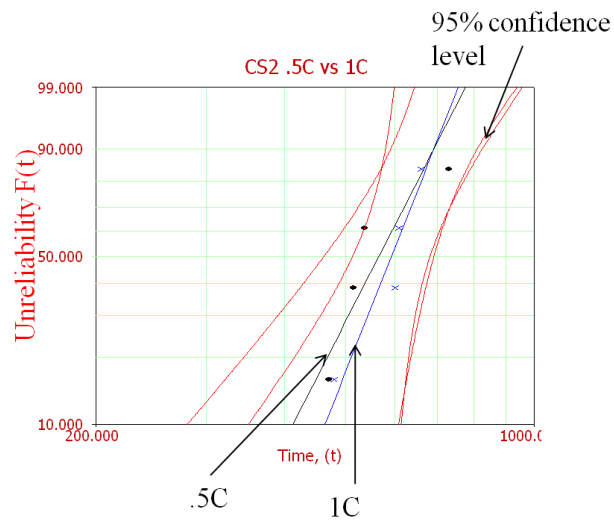


Figure 25 Weibull plot CS2 time to failure, 0.5C vs. 1.0C

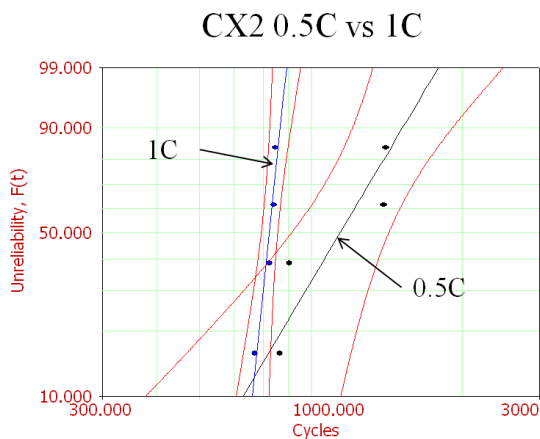


Figure 26 Weibull plot of CX2 time to failure, 0.5C vs. 1.0C

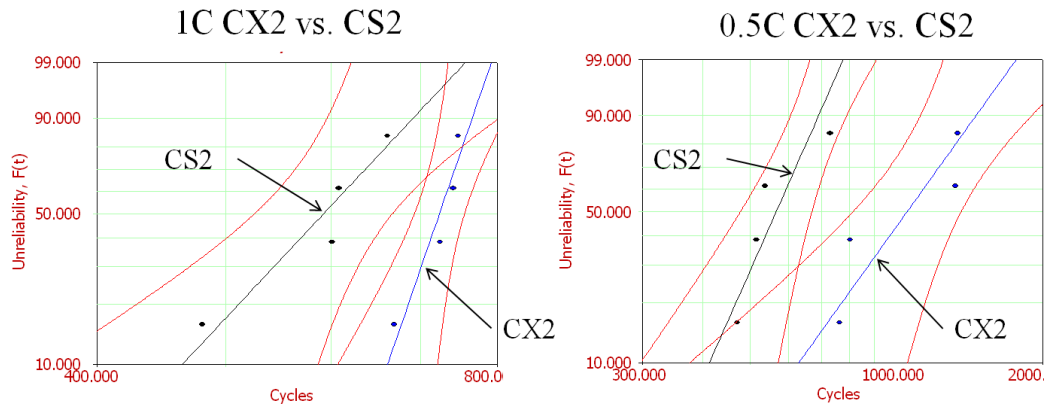


Figure 27 Comparison of CX2 and CS2 for both 0.5C and 1C discharge rates

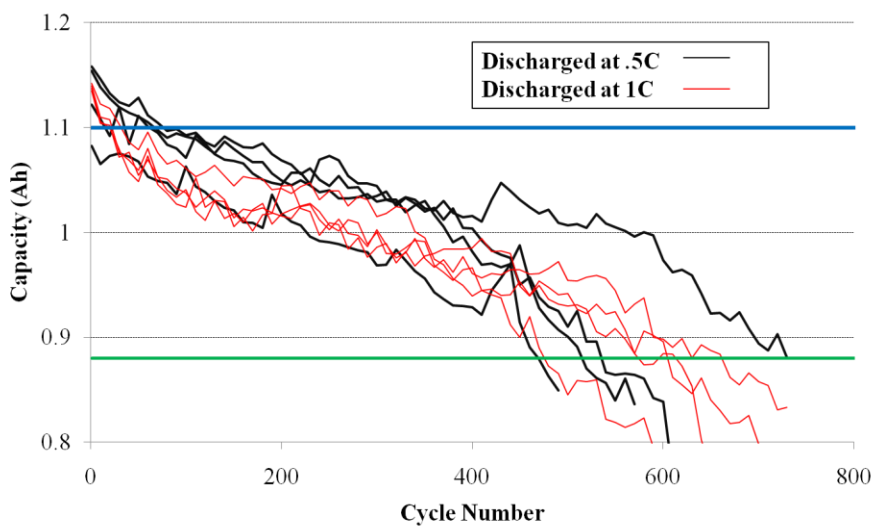


Figure 28 Discharge curves for CS2 batteries used in constant current discharge cycling test

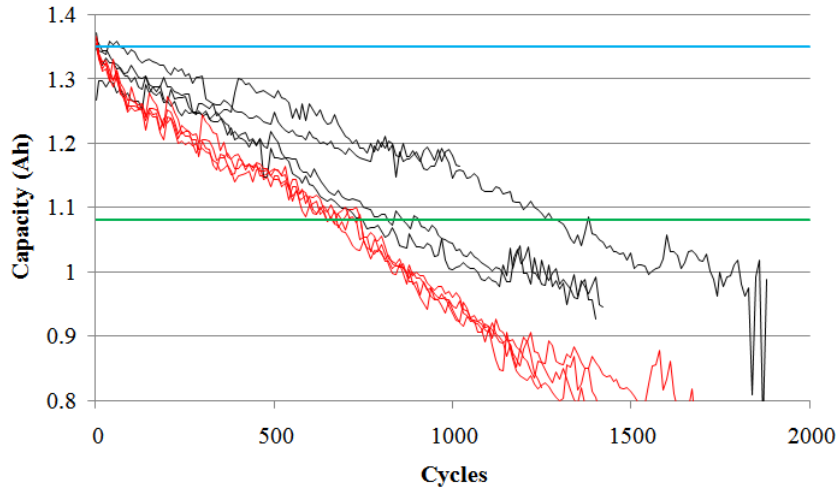


Figure 29 Discharge curves for CX2 batteries used in constant current discharge cycling test

High Rate Discharge Test

The high rate discharge test evaluated each battery's ability to deliver current at 3C while still maintaining an acceptable capacity. As discussed previously by Peukert's law, a battery experiences losses in capacity as the discharge current increases due to certain rate limiting factors such as the charge transfer resistance and the diffusion through the porous separator. Because the tested batteries are all meant for portable electronics rather than high power applications, they were not intended for use above C-rates of 1.5 or 2C, therefore their performance cannot be compared to batteries designed for high power applications which are sometimes designed to supply current rates of up to 20C.

Figure 30 shows the discharge profiles for CS2 and CX2 at the beginning of life under discharge currents of 3C, 1C, and 0.5C. The vertical black lines indicate the expected time of discharge of the batteries if there were no losses due to current rate. While the tested batteries either matched or exceeded the expected discharge capacities at 1C and 0.5C, they fall short at a discharge rate of 3C. The CS2 battery experienced a 66% loss of capacity at 3C

as compared to the capacity observed at 0.5C while the CX2 battery only lost 7% of its capacity at 3C as compared to the 0.5C discharge. This result indicates that the CX2 battery may be better suited for high rate discharge applications.

Figure 31 shows the cycle life profile for both the CX2 and the CS2 batteries. Periodically the batteries were discharged at a 0.5C to evaluate the degradation of the battery's low current rate discharge capacity due to cycling at 3C. It can be seen (by the data points in blue) in both batteries that there is a large variation (scatter) in the 3C capacity with cycle number. This is likely due to the constant build up and corresponding diffusion of solid precipitates which form on the surface of the electrodes during cycling. This is similar to the phenomenon observed during the capacity recoveries noticed during the constant current discharge test, however at higher discharge rates, these precipitates form and dissolve in much higher quantities and at much faster rates.

In the CS2 battery it is observed that the capacity fade at 3C occurs at a different rate than the capacity fade at 0.5C. At the beginning of life the 3C discharge resulted in a 66% loss of the 0.5C capacity where after 2500 cycles, there was a 90% loss of the capacity 3C discharge capacity as compared to the 0.5C discharge capacity. This means that even though a battery may have experienced failure at a 3C discharge rate, it still may be an acceptable power source when used at lower currents.

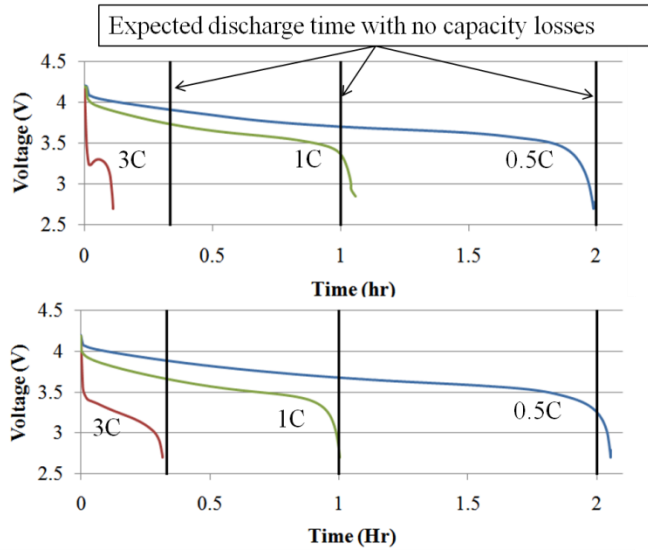


Figure 30 Discharge voltage profiles for CS2 and CX2 at 3C, 1C, and .5C discharge rates

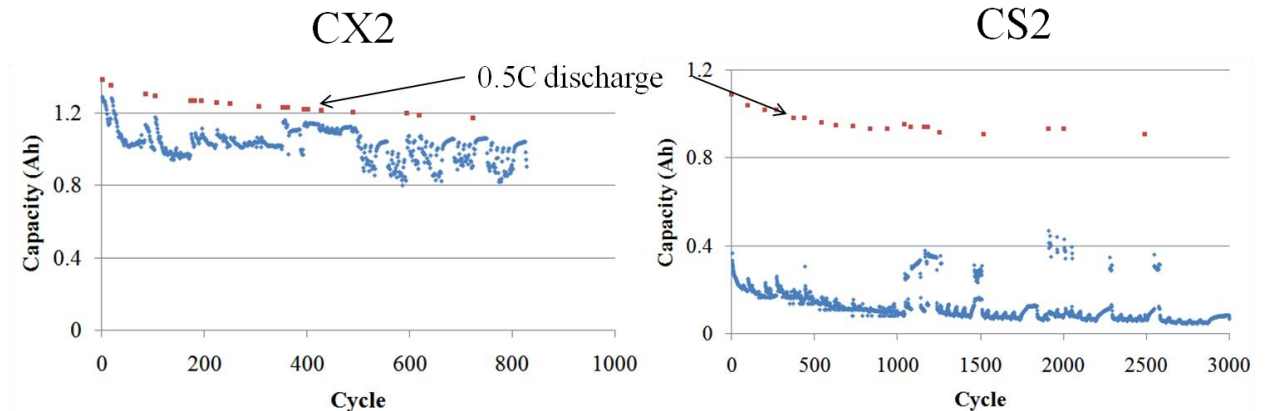


Figure 31 3C cycle life for CX2 and CS2 with periodic discharges at 0.5C (shown in red)

Pulsed Discharge Test

In many real life battery applications constant current discharges are rare. In cell phones, batteries often undergo current pulses at high frequencies known as GSM pulses (Global Standard for Mobil Telecommunication) in order to send and receive RF signals. In addition to the current draw for RF communication, new smart phones are conducting other processes

such as data base and file access, application processing, and display graphics processing that draw additional and varying current based on activity. This leads to highly complex discharge profiles. In order to begin investigating battery behavior under varying discharge conditions a simplified discharge profile was used that pulsed between 1C, 0.5C, and 0C each for 30 seconds. The current and voltage profile is shown in Figure 32, where the blue box shows a zoomed in view so the individual current pulses and voltage response can be seen.

The capacity for the pulsed current test was calculated in the same way as the constant current discharge tests. Figure 33 shows the capacity fade curve for the CX2 battery used for the pulsed discharge test compared with CX2 batteries used for the 0.5C and 1C constant current discharge test. Although the average discharge level was 0.5C, the capacity fade of the combined current pulses degrades slower than either one of the constant discharge current profiles. This could be due to the 30 second rest period that occurs between each pulse which may allow the battery to remain close to a stable electrochemical equilibrium.

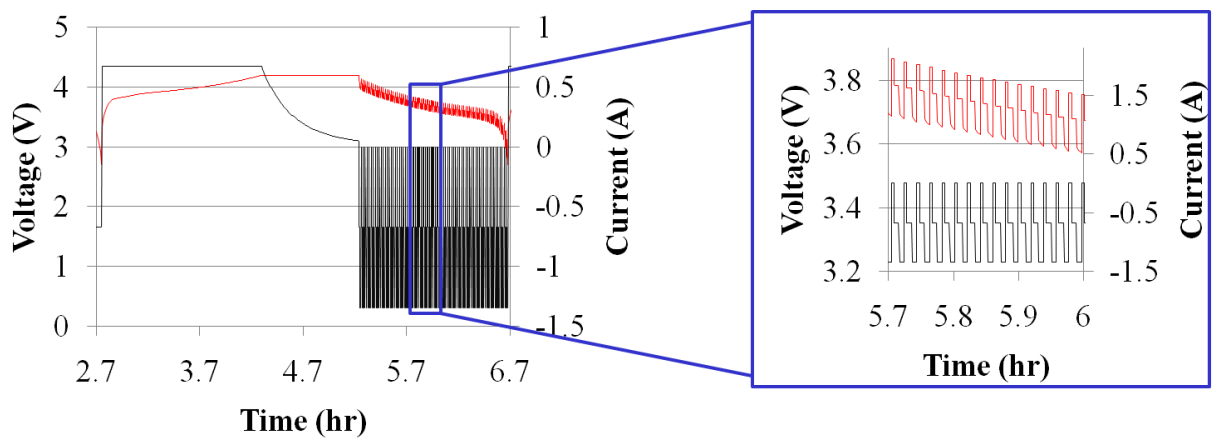


Figure 32 Current and Voltage profile for pulsed current discharge test

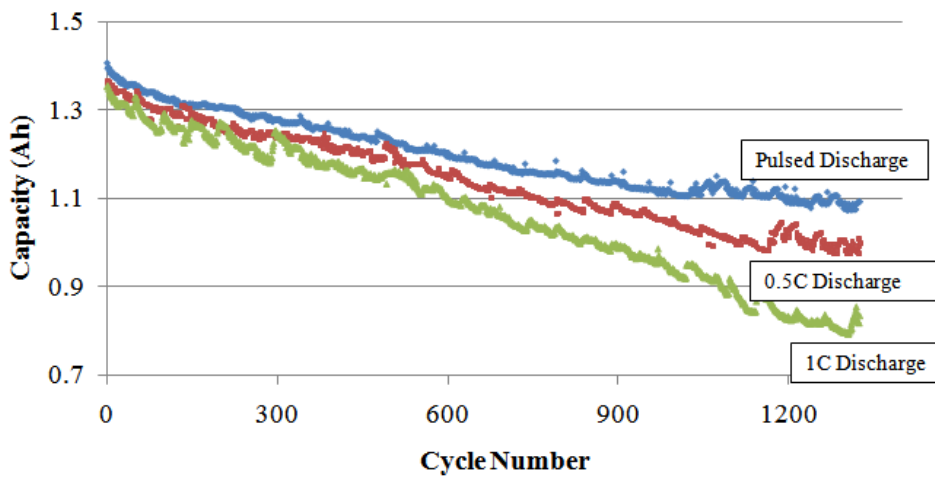


Figure 33 Capacity fade curve shown for the pulsed discharge test compared with capacity fade curves from the constant current discharge tests for 3 CX2 batteries

Continuous Charging

The continuous charging test was performed on an “A” battery to examine the effects of float charging on battery reliability. The cell subjected to this test was given a float charge at 4V for an extended period of time and was periodically discharged to measure capacity. A float charge refers to a low current charge which counteracts the battery’s self discharge effects. The float charge allows the voltage to remain constant over the duration of the rest time. Figure 34 shows voltage vs. time plots collected during various discharge times throughout the continuous charging test. There was no significant change in capacity during the continuous charging times. In a previous study [14], extended periods of float charging at voltages above 4.2V resulted in accelerated capacity fade. This is likely cause by the instability of the cathode material at higher voltages. Because the float charge in this test

allowed the battery to remain within the battery's stable operating region below 4.2V, no significant degradation was observed. This would be an important consideration for BMSs that wish to keep a battery maintained during down time. By applying a float charge in the battery's stable operating voltage, the battery can remain fully charged and ready for immediate use without undergoing significant degradation during storage.

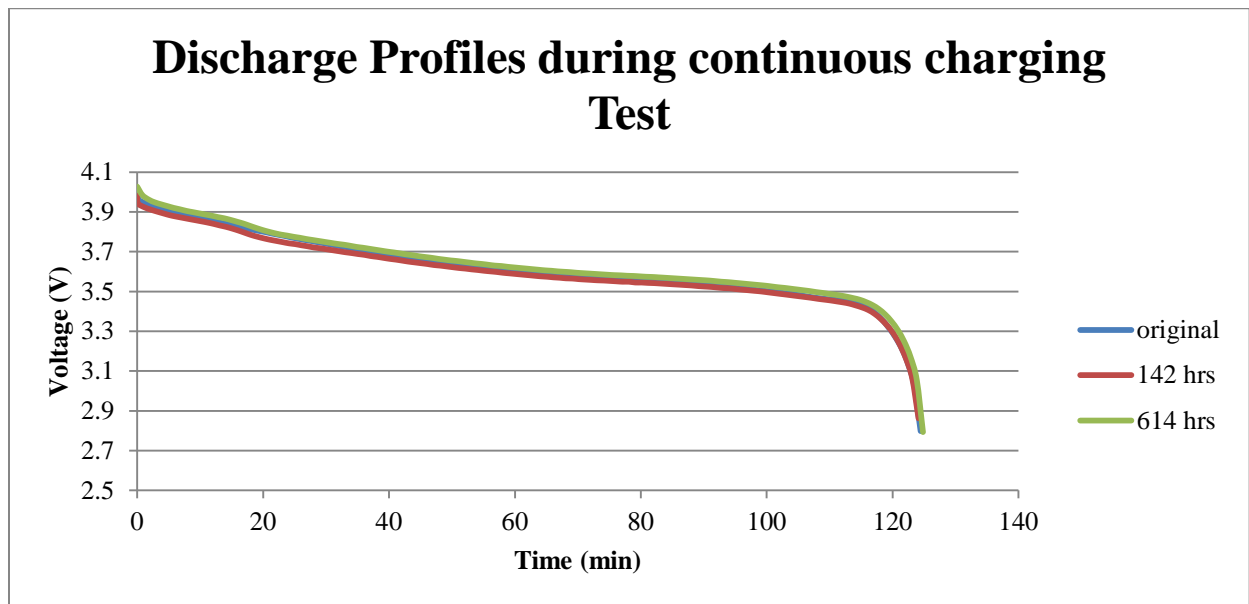


Figure 34 Voltage vs. time plots at different stages throughout the continuous charging test

Shallow charging

For the shallow charge test, an “A” battery was used. Figure 35 shows the capacities that were calculated during each discharge cycle of the shallow charging test. Only about 7% of the battery's rated capacity was utilized during shallow charging. The state of charge (SOC) of a cell is related to x in Li_xC_6 or Li_xCoO_2 [85] [86]; thus, when a battery undergoes a shallow cycle, only a fraction of Li within the cell is required to reach the necessary charge

potential. In the case of shallow charging where the charge potential is reduced, less lithium intercalation into the anode occurs. Because much less charge transfer is required to reach the potentials of shallow cycling, the time required for cycling, and thus the capacity, are drastically reduced. The first shallow cycling specimen was exposed to over 900 cycles at a voltage range of 2.75V to 3.7V. The capacities collected demonstrated a large statistical variance; however, there did appear to be a general trend of decreasing capacity. There were two recoveries in capacity observed during shallow charging, one around the 280th cycle and the other around the 700th cycle. Upon investigation of this phenomenon it was found that during these times the test had been paused for a number of hours for routine maintenance. The recovery while the battery was in an open circuit state suggests that the fade in capacity observed was not a result of irreversible consumption of active material but a buildup of solid precipitates on the electrode surface that were allowed to diffuse back into the electrolyte solution while the battery was not cycling.

No significant degradation was observed after 900 shallow charging cycles. This is not to say that an indefinite number of shallow charging cycles would never result in a battery failure, but in general the “A” batteries displayed failure times of under 300 cycles for full discharge cycles at the same current rate. Thus, notwithstanding 900 shallow discharge cycles without a drop in performance suggests that the degradation caused by shallow cycling is minimal. To further investigate the health of the shallow charged sample, the battery was allowed to be cycled under the conditions outlined for the constant current discharge cycle life test. The first full discharge cycle after shallow charging yielded a capacity of .921Ah, which was higher than the capacity recorded during the baseline measurement taken before shallow charging began confirming that the shallow cycling caused little degradation to the cell.

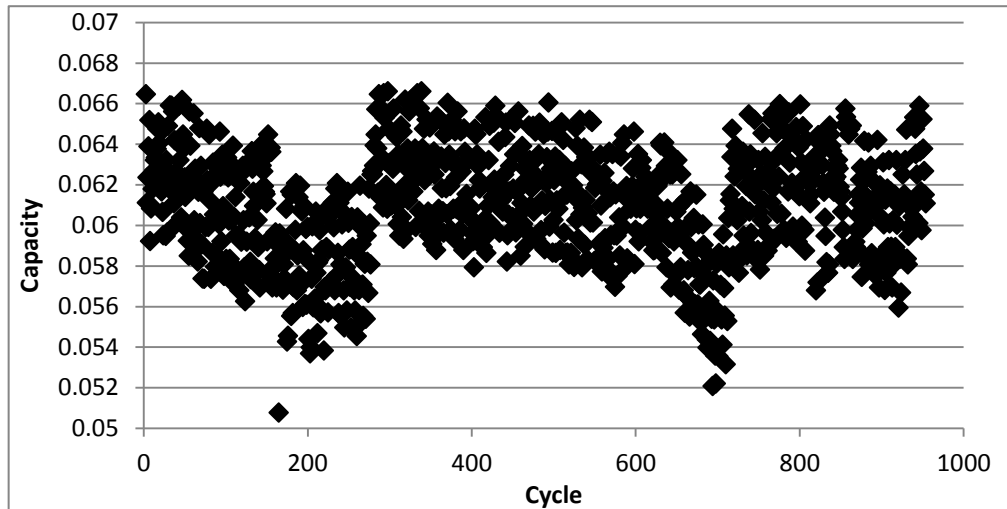


Figure 35 Cycle vs. capacity for shallow charging battery

Figure 36 shows the capacity curve for the sample after it was removed from shallow charging and cycled under constant current discharge conditions. The sample is compared with a cell that saw no shallow charging pre-conditions. Both curves display a gradual linear degradation prior to a more rapid loss in capacity. While the cell exposed to shallow charging retained its liner phase for slightly longer than the fresh cell more testing would be required to determine if that was due to the shallow charge cycles.

Around the 80th cycle there was a discontinuity observed in the shallow charged cell. Capacity made a permanent drop from 0.86Ah to 0.80Ah. This drop did not seem to have had any effect on the slope of the linear region other than to shift the curve down. This phenomenon is not related to the growth of SEI layer or breakdown of electrolyte solvents, because those factors cause a gradual decline in capacity fade. The sudden drop may be attributed to a fracture of one of the electrodes, which could possibly have been caused by electrode misalignment, native contamination, or pouch seal-fold impingement [87]. It is also possible that the shallow cycling, even though there were no noticeable effects on capacity

fade, could have caused small structural changes in the electrodes (such as micro cracks) which lead to a sudden fracture during the full discharge cycles.

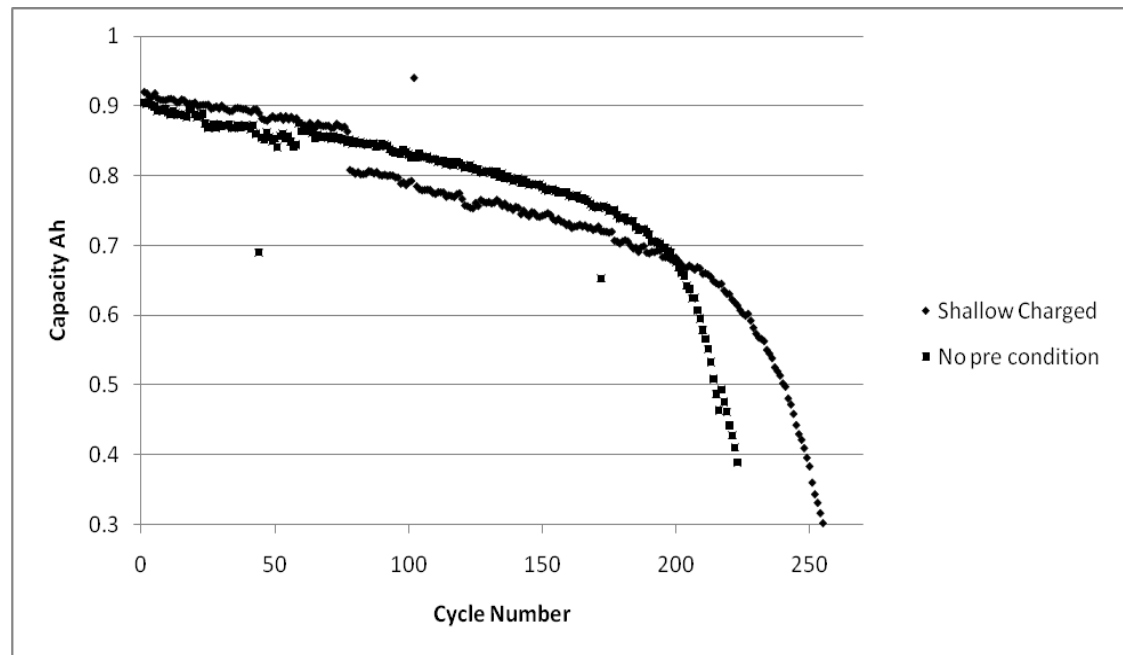


Figure 36 Capacity vs. cycle number comparing an “A” battery that was shallow charged for 900 cycles as a precondition and an “A” battery that had no prior usage

Self Discharge

Batteries that were tested for self discharge qualities showed a rapid drop in open circuit voltage after the first hour of being removed from the charger. After the first hour batteries displayed a steady decrease in open circuit voltage of about 1% drop per month. This is shown in Figure 37 which shows the open circuit voltage vs. rest time for an “A” battery. This battery had not undergone previous cycling. Results from Sun Hee Choi [84] between nanocrystalline LiCoO_2 and coarse-grained LiCoO_2 indicated improved self discharged characteristics from batteries with developed SEI layers. These results suggest that batteries that were previously cycled might have lower rates of self discharge than brand new batteries due to the advanced SEI insulation layer on the anode.

In order to investigate the effects of the SEI layer on self discharge, a CX2 battery was exposed to constant current discharge cycling at .5C. Periodically the test was halted and the battery was charged to 4.2V and left to rest without a discharge load. The open circuit voltage was monitored so that the rate of self discharge could be observed. Figure 38 shows the self discharge curves for a CX2 battery at different points in its cycle life. It is interesting to note that towards the beginning of the battery's life (cycle 0 and cycle 34), the voltage drop that occurs after the battery is removed from charging is relatively large. This time period corresponds to the first stage of capacity loss or the formation period. At this point a stable SEI layer has not yet covered the electrode surface and electrons are not well insulated in open circuit conditions. The drops in voltage at cycles 226 and 300 are much smaller as these correspond to the second stage of capacity loss when a stable SEI acts as a passivation layer over the electrodes. This insulates electrons preventing a high degree of self discharge. At cycle 600, the drop in voltage due to self discharge is again relatively high. This could be due to the fact that constant cycling resulted in mechanical damage to the electrodes. The cracks in these electrodes allow active material to become exposed to the electrolyte creating a pathway for electrons to migrate from the anode back to the cathode.

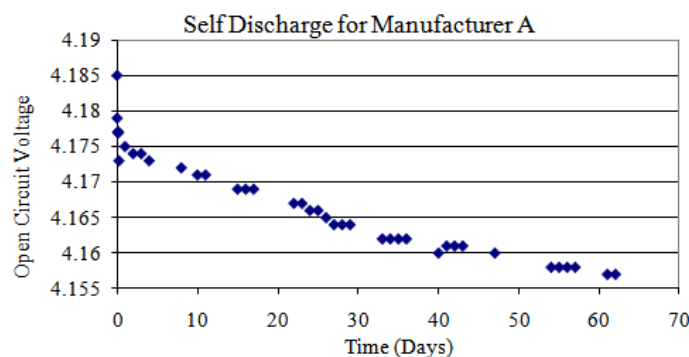


Figure 37 Self discharge curve for an “A” battery

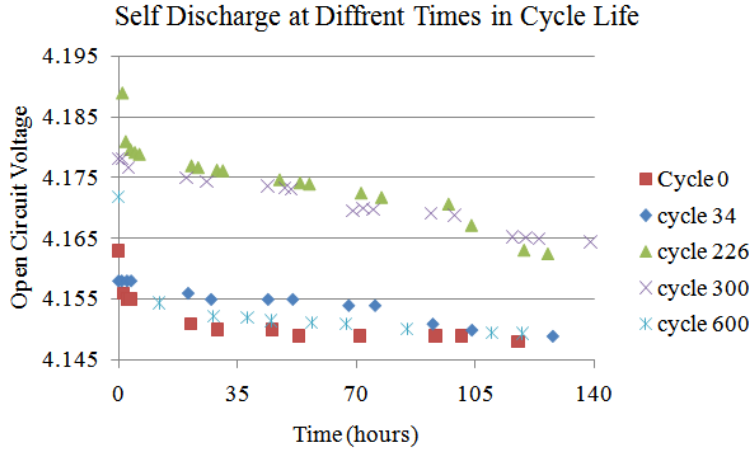


Figure 38 Self discharge for a CX2 battery at different points during its cycle life

Random Cut-off Voltage Test

The random cut-off voltage test provides a close simulation to actual usage conditions, as cycling is not always conducted to the exact same depth of discharge (DOD) during every cycle. Varying the discharge cut-off voltage leads to a problem during the degradation analysis because the value of Q_{\max} is not directly measured. Therefore the state of health (SOH) of the battery becomes harder to analyze. In order to solve this problem, of evaluating SOH using the information obtained during partial discharges, a method is described below. This method is then evaluated on the data generated from the partial discharge test.

Mathematically, SOH is a normalized measure of Q_{\max} . It is normalized with respect to the rated capacity (Q_{rated}) which is a constant determined by the manufacturer to give the user an indication of how much charge a specific battery model will be able to supply in a single discharge. At the beginning of life $Q_{\max} \sim Q_{\text{rated}}$. As a battery is cycled or aged, Q_{\max} begins to decrease and so SOH can be determined by:

$$SOH = \frac{Q_{\max}}{Q_{\text{rated}}} \times 100\% \quad (2)$$

As described in the introduction section, Q_{\max} cannot always be expected to be directly measured due to unpredictable user discharge profiles. Therefore, in field applications, current and time data will most often be used to calculate Q_c , which is the capacity calculated during any particular discharge cycle. This value will be subjected to large fluctuations depending on the DOD of any particular discharge and therefore will not be equal to Q_{\max} . Q_c must be calculated using sensor data which will be collected with n number of samples. Therefore to calculate Q_c during any particular discharge we use:

$$Q_c = \sum_{i=1}^n (I_{i-1} + \frac{I_i - I_{i-1}}{2}) t_i \quad (3)$$

where I is current in Amperes, t is the time in hours between each particular sample, i is a particular sample and c is the cycle counter.

At the end of each discharge cycle, i.e. when the current supplied by the battery switches from a negative value to a positive value, the open circuit voltage recorded is V_d and:

$$V_d \in [V_{\text{discharge}}, V_{\text{charge}}] \quad (4)$$

where $V_{\text{discharge}}$ is the manufacturer recommended discharge cut-off voltage and V_{charge} is the manufacturer recommended charge cut-off voltage. If:

$$V_d = V_{\text{discharge}} \quad (5)$$

Then:

$$Q_c = Q_{\max}^c \quad (6)$$

If not then Q_c must be converted into a form that can be compared to Q_{\max} . During controlled battery cycling tests, charge and discharge profiles are normally all conducted with the same cut-off voltage; Thus when a decrease in capacity is observed, it can be attributed to

degradation phenomena occurring within the battery. If battery cycling is conducted where each particular discharge cycle is cut-off at a random voltage, then changes in capacity would be mostly attributed to DOD and the contribution from battery degradation would be lost in the noise. Because SOH is concerned with battery degradation and not DOD it makes sense to only calculate SOH based on the rate of capacity fade between capacity values that were determined between the same cut-off voltages. In literature $V_{\text{discharge}}$ is most often used as the cut-off voltage during testing so that SOH can be calculated in terms of Q_{rated} [88,14]. However if we adhere to the assumption that changes in capacity measured at the same cut-off voltage are indicative of battery degradation (rather than DOD), then the rate of change of any two capacities evaluated at the same cut-off voltage, can be used to identify the rate of change in the battery's SOH. Because we still want to evaluate SOH in terms of Q_{rated} we can introduce a term $Q_{\text{equivalent}}$ which assumes the value of Q_{\max} but degrades at a rate indicated by two comparable Q_c values. So for any two Q_c evaluated at equivalent V_d values:

$$Q_{\text{equivalent}} = (Q_{\max}^{c-1}) \left(1 + \frac{dQ_c}{dc} \right) = Q_{\max}^c \quad (7)$$

Where dQ_c is the difference in capacities of any two cycles that were evaluated over the same voltage range and dc is the difference in cycle number of the two capacities being evaluated. $Q_{\text{equivalent}}$ can now be applied to both data points used in the comparison. In effect, $Q_{\text{equivalent}}$ estimates what the battery capacity would have been, had it been fully discharged to 100% DOD. It should be emphasized that the Q_c values used to evaluate $Q_{\text{equivalent}}$ do not need to be consecutive. $Q_{\text{equivalent}}$ should be evaluated using the two nearest Q_c values with the same cut-off voltage even if there are several other cycles in between them. Also in order to further reduce noise, dQ_c/dc could be taken as the average rate of change of many “similar” discharge cycles if it is available in the data.

In order to correctly interpret this data, each updated Q_{\max} value should be normalized with respect to Q_{rated} so that the data is shown in the SOH range. Also, due to the way this data was processed, these SOH values exist in the cycle domain. Because each cycle interval is considered equivalent, time information is lost. In order to overcome this and make meaningful remaining useful life predictions, each cycle should be interpreted as an average user cycle where the time of each cycle is calculated by:

$$\bar{t} = \frac{\sum_{k=1}^c (\sum_{i=1}^n t_i)_k}{c} \quad (8)$$

where i is a sample and k is a cycle number. Using this value, future predictions in the cycle domain can easily be converted to the time domain by simply calculating \bar{t} at the time of prediction. The value however must be recalculated before every prediction because it will change based on the users typical usage behavior.

Figure 39 provides a simple schematic as to how this method will combine capacity measurements. Consider a battery that is discharged to four different cut-off voltages, each one applied throughout a quarter of the battery's cycle life. The lines shown in Figure 39 represent the trend fit to the capacities in each voltage regime. Because the cut-off voltage influences the calculated capacity, there will be discontinuities between each of the four sections; however each section still provides some information as to how much capacity was lost during cycling. By relating these capacities though the equivalent Q method we can better track degradation and eliminate the noise caused by differences in DOD.

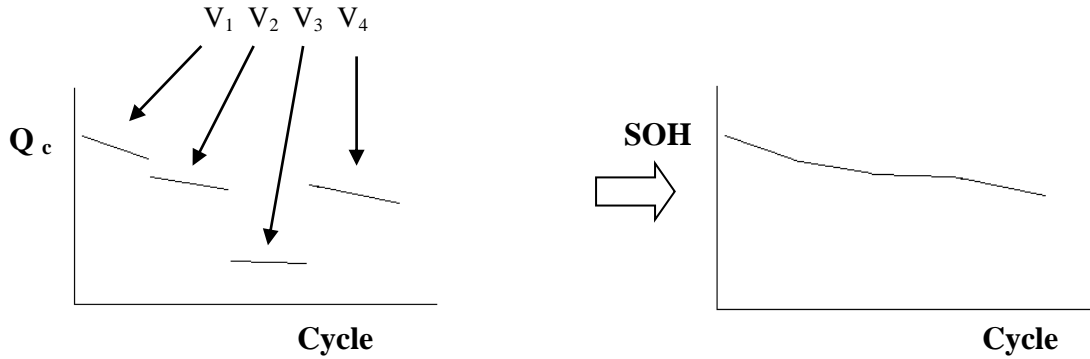


Figure 39: A schematic demonstrating the results of applying the Q equivalent method to a battery discharged at 4 different DOD during its cycle life

In order to validate this methodology, an algorithm was written in Matlab to analyze the data from the partial discharge test and evaluate the equivalent Q_{\max} values for each partial discharge. The algorithm searches the data to group together all the discharge cycles that could be considered similar to each other. For example if the similar criteria were 0.1V, all the discharge cycles that had cut-off voltages within 0.1V of each other would be considered similar and the rate of change of these capacities with their respective cycle number could be used to evaluate the rate of change of the maximum capacity. When the rate of change of the maximum capacity was evaluated for every cycle, the battery's degradation curve could be plotted because the dQ/dc would be known for every cycle and the original Q for the first cycle could just be assumed to be the rated capacity.

Figure 40 shows the equivalent Q along with the observed capacities. The points in red show the observed capacities for each cycle. These points have such large variations due to the random changes in cut-off voltage every 15 cycles. The change in cut off voltage effects the discharge time and hence the capacity also changes. The blue points show the equivalent capacity that is calculated using the method described above. It can be seen that this provides a good estimation of the maximum discharge capacity for each cycle, even for those cycles that are not completely discharged. At cycle 1000, the battery was fully discharged to its cut-

off voltage, therefore the algorithm recalibrated its Q_{\max} value to the value observed from testing. This recalibration explains the drop in capacity at cycle 1000.

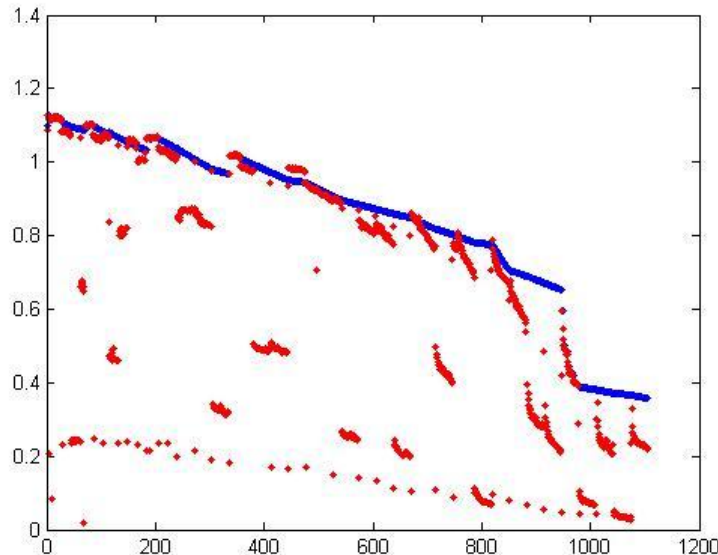


Figure 40 observed capacities are shown in red, and the predicted maximum capacity based on the equivalent capacity method is shown in the blue

Failure Analysis Results

Failure analysis was conducted on each type of battery to investigate the physical mechanisms of degradation. Most of these methods were conducted after cycling so that disassembly could be conducted, however impedance spectroscopy measurements were able to be performed in situ. These methods are described below.

Impedance Spectroscopy Measurements

Using a Solartron Mobery SI 1287 Electrochemical Interface to record impedance measurements at frequencies ranging between 1mHz and 1MHz, we were able to produce and compare Nyquist plots at different times during a battery's life cycle.

Figure 41 shows the Nyquist plots of a CS2 battery taken at various cycle points over the course of the cycle life test. Each plot is displaced on the real axis; however, the displacement does not correspond with a continuous increase in cycle time. This may indicate that cell morphology causes impedance to fluctuate during cycling [21][22]. The displacement along the x-axis of the Nyquist plot (where the curve first crosses the x-axis) is indicative of the electrolytic resistance. We find that the electrolytic resistance at cycle 500 is similar to the electrolytic resistance at the 46th cycle suggesting that even after 500 cycles, the electrolyte conductivity did not undergo significant degradation. However, the width and the height of the semi-circle underwent a major increase on the 500th cycle. This is indicative of an increase in charge transfer resistance (as indicated by the second point where the semi-circle crosses the x-axis) and double layer capacitance which can be found by identifying the very top part of the circle and calculating:

$$w_{max} = 1/C_{DL}R_{CT}$$

where w_{max} is the frequency at the top of the semi-circle, C_{DL} is the double layer capacitance, and R_{CT} is the charge transfer resistance. This Nyquist plot evolution suggests that the degradation in this battery can be attributed by increased impedance at the electrolyte/electrode interface. The mechanisms responsible for increased impedance at this interface are increasing thickness of the SEI layer and increased resistance in the solid (electrode) phase of the battery (due to mechanical damage and decreased adhesion between electrode particles). Figure 42 shows the corresponding capacity fade for the EIS measurements taken from the battery. It can be seen that around the 500th cycle there is a sharp increase in the rate of capacity fade which can be explained by the degradation mechanism inferred from the EIS data.

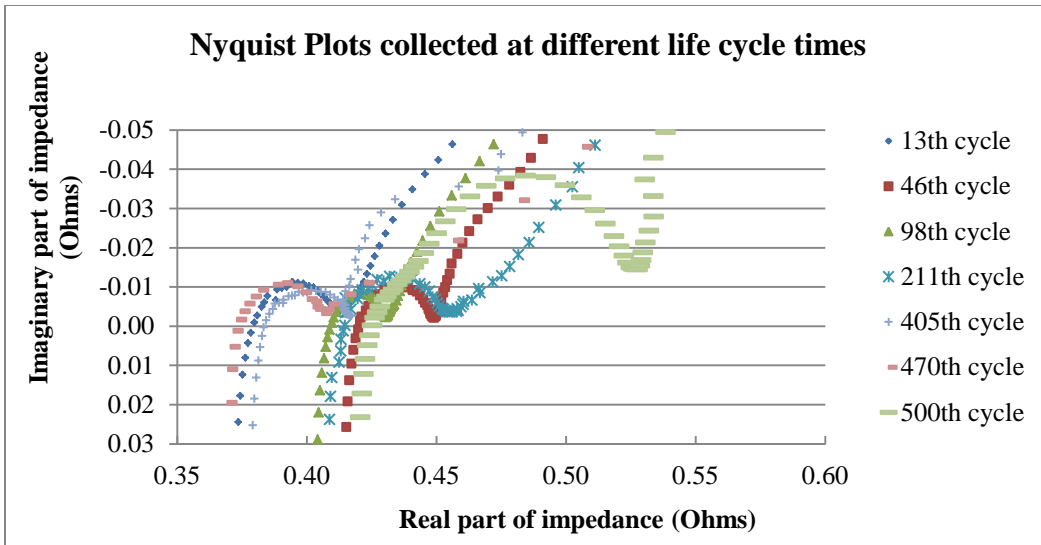


Figure 41 Impedance measurements taken periodically though life of CS2 battery

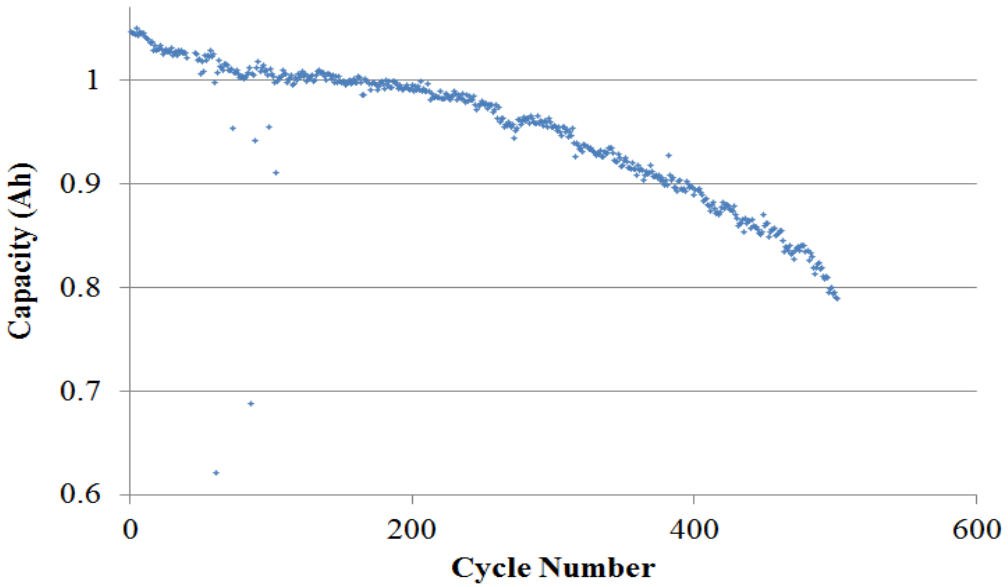


Figure 42 Corresponding capacity fade for the above impedance measurements for CS2 battery

Figure 43 shows a battery from Manufacturer A that was cycled at manufacturer-recommended conditions. Unlike the previous sample, this battery does show a large

displacement on the x axis as cycle number increases. The Nyquist plot recorded after 165 cycles in Figure 43 shows that both the electrolyte resistance as well as the resistance at the electrode interface was responsible for the degradation of this battery. In Figure 41 CS2 cell does show a sharp increase in impedance at cycle 500 as indicated by the dramatic increase in the semi-circle radius however it differs from the manufacturer A cell because the electrolytic resistance remains consistent with most of the previous measurements. These results indicate that electrolyte decomposition was a larger factor in the degradation of the “A” battery as compared to the CS2 battery. Future work can investigate the compositional differences between both electrolytes to determine the weaknesses of the “A” battery’s electrolyte mixture.

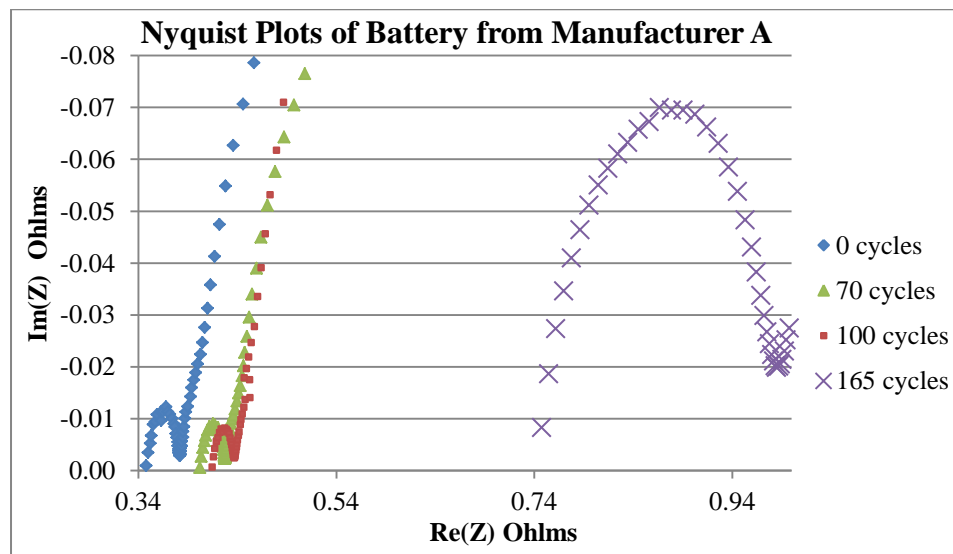


Figure 43 Impedance measurements taken periodically through life of an “A” battery

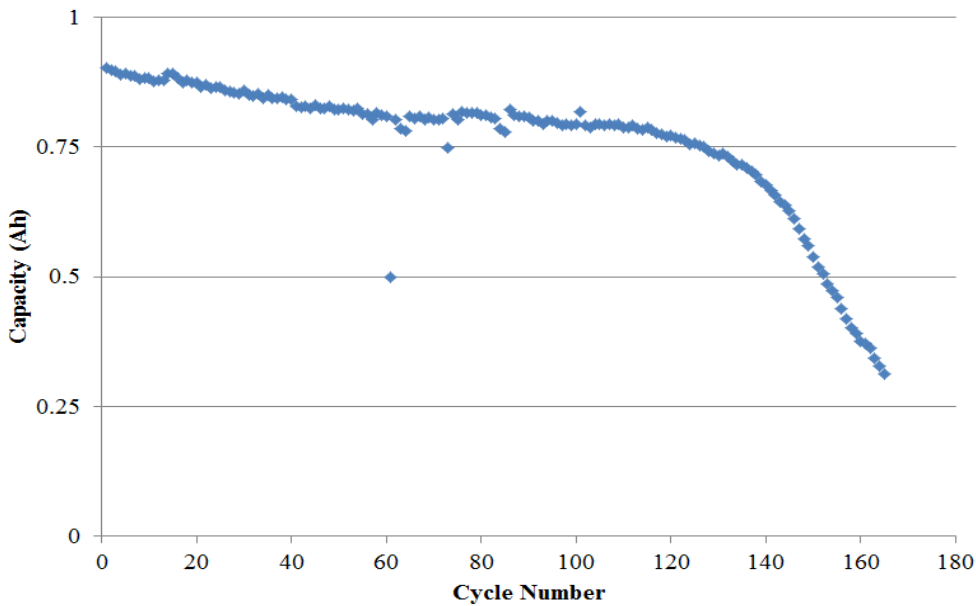


Figure 44 Capacity fade curve corresponding to the above Nyquist Plots for an "A" battery

Tape Pull Test

In order to test the coherence and adherence of the electrodes to themselves and to their respective current collectors, the tape pull test was employed. This method is often used to test solder mask and plating adhesion and it is described in standard IPC-TM-650. Following the procedures outlined in this standard, this test was applied to battery electrodes using 3M Scotch 371 tape which was described to have adhesion strength of 44 N/100 mm.

For the tape pull test two CS2 batteries were used. One of the batteries was considered failed and the other was considered new. The failed battery had undergone the 0.5C constant current discharge test for 500 cycles and had experienced a 25% reduction in capacity. The new battery had not undergone any charge/discharge cycling. Both batteries were disassembled using the methods described in the “disassembly” section and the tape pull test was performed on the anode and cathode of both batteries.

Figure 45 shows the results of the tape pull test. The four photos on the left side are images of the tape after the tape pull test was performed. It can be seen that for the non-

cycled electrodes, the anode and cathode were cleanly pulled off of the current collector leaving most of the electrode material stuck to the tape. The tape pull test results indicate that the weakest interface before cycling began was between the electrodes and the current collector. For the test sample that was failed, only the top surface of the electrode material came off with the tape, while the remaining material was left on the current collectors. This was the case for both electrodes. This result indicates that, either the strength of the adhesive bond between the electrode materials and current collectors increased, or the strength of cohesion and/or adhesive bonds between the particles in the composite electrodes decreased. This could lead to two possible conclusions. The first is that particles closer to the current collector interface were welded due to microheating at contact points resulting in increased adhesion to the current collector. The second possible conclusion is that the particles making up the bulk electrode structure were not held together as well after cycling. Because these particles are held together by a polymer binder, it is likely that this binder material degrades with charge discharge cycling resulting in reduced cohesion strength within the bulk electrode. Further testing will need to be performed to conclude which of these two scenarios are more likely.

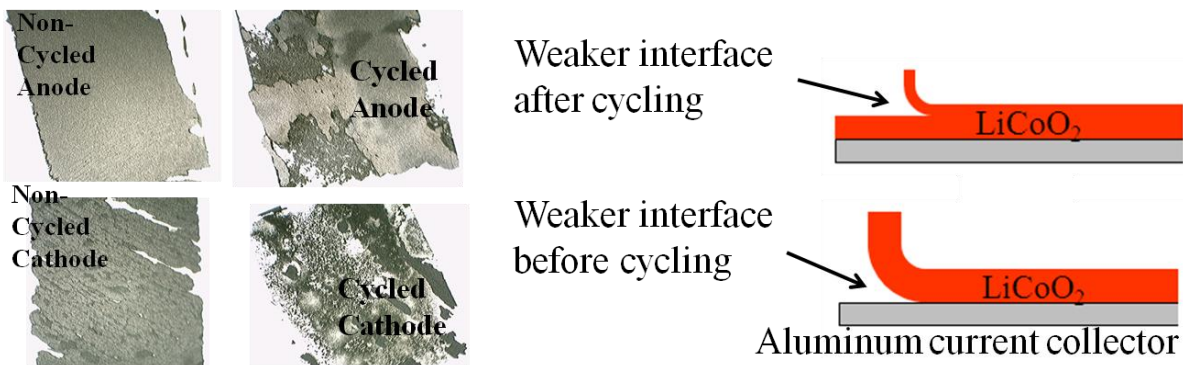


Figure 45 results of the tape pull test on electrodes of a new and cyclic tested CS2 battery. The schematic on the right shows the weakest interface observed at the time of

the tape pull testing for the cathode. Similar results were observed for the anode with a copper current collector.

Atomic Force Microscopy

Atomic Force Microscopy (AFM) is performed by applying an oscillation frequency to a small AFM tip. This tip is then slowly dragged over the surface of a material. Based on the local height of the surface material the AFM tip will undergo slightly different deflections during its oscillations. These deflections can then be back correlated to the height of the material in order to give a topological overview of the surface material.

The surface topologies of a non-cycled and cycled anode from a CS₂ battery are displayed in Figure 46. The cycled anode and undergone the 0.5C constant current discharge test for 500 cycles and resulted in a 25% decrease in the nominal capacity. The images depict a higher surface area with a higher number of surface peaks for the non-cycled anode compared to the cycled anode. Graphite has a stacked ABA lattice structure with a layered and almost flakey characteristic to it. Lithium ions insert themselves into these layers of graphite which provides the mechanism for energy storage. The more surface area of the graphite that is exposed to the electrolyte the more lithium that will be able to be inserted during cycling.

The cycled electrode appears to have smaller and more rounded peaks and therefore less surface area available for lithium insertion. This smoothing could have been caused by a buildup of surface films on the electrode surface. This could be an effect of electrode expansion and contraction which leads to the changes in the surface topology. Specifically damaged anode particles become detached from the bulk electrode and dissolve into the electrolyte solution. This would lead to uneven density of material in the electrode causing a non-uniform flux of intercalated lithium over the anode's surface. Differences in local strains due to uneven lithium insertion will lead to the formation of micro-cracks during cycling.

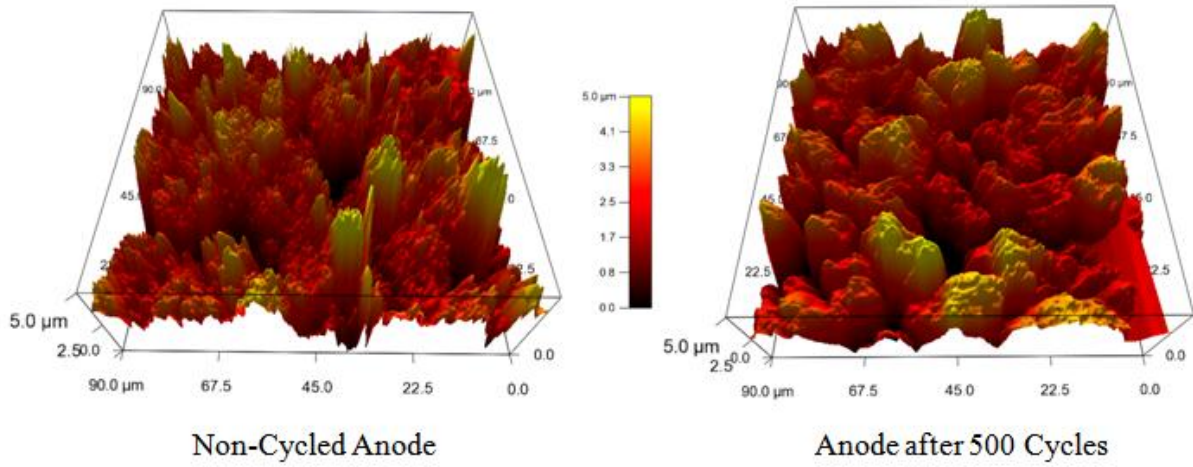


Figure 46 topography maps of CS2 anode by AFM

Scanning Electron Microscope

The environmental scanning electron microscope (ESEM) provides a good method to look closely at the disassembled battery materials to observe the degradation mechanism that results in capacity fade. Figure 47 shows an image after the tape pull test of a cycled CS2 anode. The image on the left was taken on the surface of the anode that was exposed to the electrolyte, while the image on the right was taken on the surface that was facing the current collector (on the surface of the tape after the tape test was performed). Upon examination, the SEI layer (left image) can be seen providing a thin surface film over the electrode. On the right image, which was not directly in contact with the electrolyte, the grainy jagged edges of the graphite electrode can be seen much clearer as no film has formed on this surface.

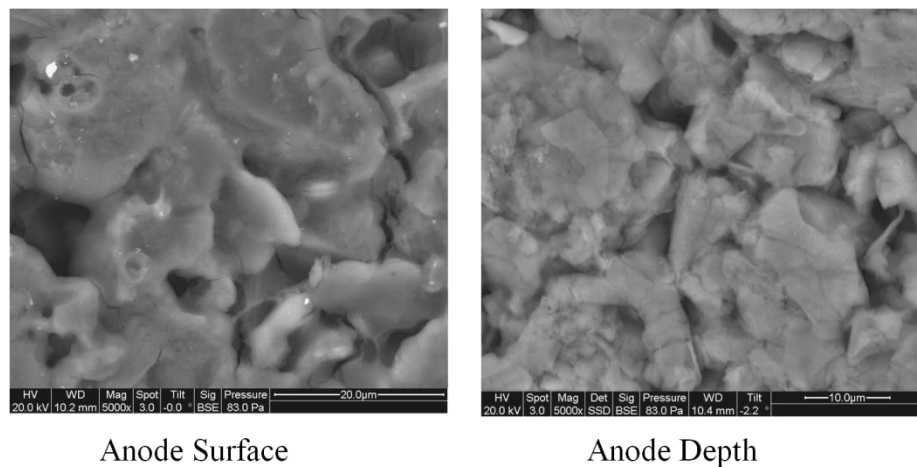


Figure 47 Anode images shown at the surface and at the underside of the the battery electrode

An ESEM image and corresponding EDS mappings of the cathode of a CS₂ battery are shown in Figure 48. From this image it can be seen that the surface films that form on the cathode occur in much more localized regions rather than uniformly over the entire surface as is the case in the anode. EDS mappings of the darker spots on the electrode reveal the presence of phosphorous which likely indicate Li_xPF_y and Li_xPF_yO_z decomposition products that occurred during cycling.

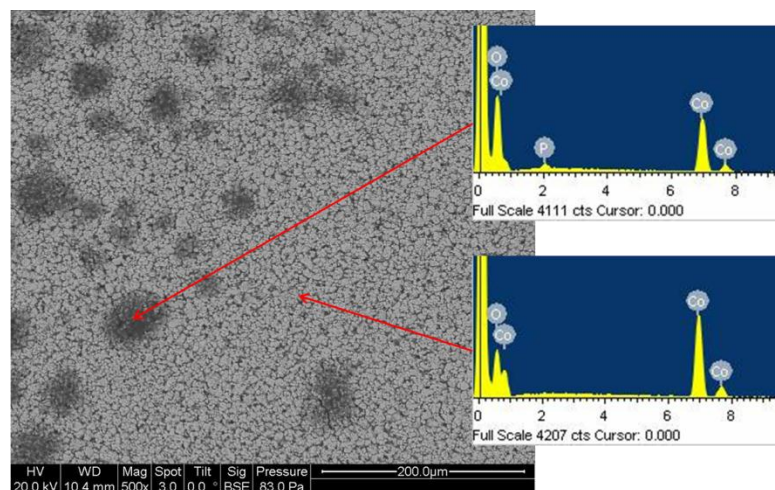


Figure 48 Cathode surface after cycling

A closer look at the cycled cathode as compared with a non-cycled cathode in the CS2 battery reveals cracks in the particles making up the LiCoO₂ shown in Figure 49. This is evidence of mechanical damage likely from expansion of particles perhaps due to lithium intercalation.

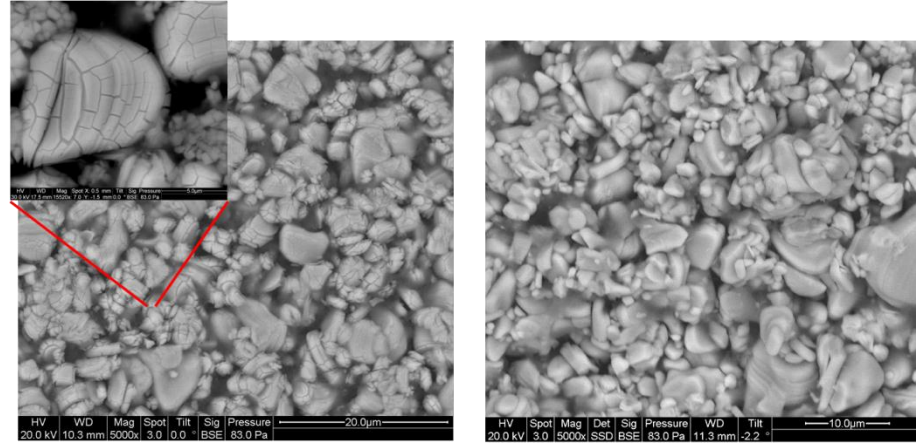


Figure 49 cycled and non cycled cathode

5. Conclusions

This thesis presents a study on the performance, reliability, physical degradation, and analysis of lithium-ion batteries. A disassembly method was developed which considers the effects of the outside environment on exposed battery materials once they have been removed from their hermetically sealed cases. It was found that oxygen and water moisture from the environment and thermal and mechanical damage due to improper disassembly can have property altering effects on battery electrodes. The proposed method considers these effects and minimizes them in order to produce failure analysis results that reflect the nature of the battery materials prior to disassembly.

Capacity vs. cycle number was analyzed for several cells through charge/discharge cycling to evaluate the progression of state of health (SOH) with usage. Statistical analysis was performed on cycle life data in order to evaluate the reliability of each battery type as compared to the others. In order to investigate the (often complex) effects of real-life usage conditions on battery degradation, a wide range of discharge profiles were used. A major problem with determining SOH through capacity measurements was identified when subjecting the batteries to partial discharges. This is because for partial discharges, the maximum capacity could not be identified and therefore there was no constant reference point in order to calculate SOH. To resolve this problem the equivalent capacity method was developed. The equivalent capacity method estimates the maximum capacity of a battery by assuming that the rate of capacity fade between two similar discharge profiles is equivalent to the rate of fade of the maximum capacity. Through this assumption, capacity fade and SOH can be evaluated for partial discharges.

Several methods of failure analysis were conducted on new and cycled batteries in order to understand the effects of degradation on the material level. ESEM, AFM, and optical results confirmed many of the degradation mechanisms that have been presented previously in literature [2]. These include the formation of surface films on the electrodes, mechanical damage to the electrode structure, and decomposition of the electrolyte. A novel extension of the tape pull test was demonstrated to test the adhesion and cohesion strength of the electrode particles to the current collector and to themselves. It was found that the tape pull test can identify shifts in the weakest interface due to cycling.

6. References

- 1 A. Patil, V. Patil, D. W. Shin, J. Choi, D. Paik, S. Yoon. Materials Research Bulletin 43 (2008) 1913–1942
- 2 P. Arora, R. White, M. Doyle. J. Electrochem. Soc. 145 (1998) 3647-3667
- 3 M. Verbrugge, B. Koch. J. Electrochem. Soc. 143 (1996) 600-608
- 4 H. Liu et al. / Journal of Power Sources 173 (2007) 556–561
- 5 Q. Liu, D. Mao, C. Chang, F. Huang. Journal of Power Sources 173 (2007) 538–544
- 6 M. Takahashi, S. Tobishima, K. Takei, Y. Sakurai. Journal of Power Sources 97-98 (2001) 508-511
- 7 J.-T. Lee et al. / Journal of Power Sources 173 (2007) 985–989
- 8 M. Gropper, C. Bartlett, Manufacturing lithium-ion batteries in gloveboxes vs. dry rooms and the effects on battery efficiency, safety, quality and overall production cost. (MBraun Glovebox Technology 2009), http://www.mbraunusa.com/pdf/MBRAUN-Manufacturing_lithium_-web.pdf . Accessed 10 January (2011)
- 9 M. Kotobuki et al. / Electrochimica Acta 56 (2011) 1023–1029
- 10 H. Maleki, J.N. Howard / Journal of Power Sources 137 (2004) 117–127
- 11 G. Ning, B. Haran, B. Popov, Journal of Power Sources 117 (2003) 160-169
- 12 W. Peukert, Elektrotechnische Zeitschrift 20 (1997) 20–21
- 13 D. Doerffel, S.A. Sharkh / Journal of Power Sources 155 (2006) 395–400
- 14 S.S. Choi, H.S. Lim / Journal of Power Sources 111 (2002) 130–136
- 15 P. Ramadass et al. / Journal of Power Sources 112 (2002) 606–613
- 16 D. Aurbach, B. Markovsky, A. Rodkin, M. Cojocaru, E. Levi, H. Kim. Electrochimica Acta 00 (2002) 1-13
- 17 P.Ramadass, Bala Haran, Ralph White, Branko N. Popov. Journal of Power Sources 112 (2002) 606-613

- 18 H. Ploehn, P. Ramadass, R. White. *Journal of the electrochemical Society* 151 (2004) 456-462
- 19 M.Lu, H. Cheng, Y.Yang. *Electrochimica Acta* 53 (2008) 3539-3546
- 20 J. Vetter, P. Novak, M.R. Wagner, *Journal of Power Sources* 147 (2005) 269-281
- 21 U. Troltzsch, O. Kanoun, H. Trankler, *Electrochimica Acta* 51 (2006) 1664-1672
- 22 M. Itagaki, N. Kobari, S. Yotsuda, K. Watanabe, S. Kinoshita, M. Ue. *Journal of Power Sources* 135 (2004) 255-261
- 23 H.-S. Jeong et al. / *Journal of Membrane Science* 364 (2010) 177–182
- 24 I.Bloom, B.W. Cole, J.J. Sohn, S.A. Jones, E.G. Polzin, V.S. Battaglia, G.L. Henriksen, C. Motloch, R.Richardson, T. Unkelhaeuser, D. Ingersoll, H.L. Case. *Journal of Power Sources* 101 (2001) 238-247
- 25 C. Huang, K. Huang, S. Liu, Y. Zeng, L. Chen. *Electrochimica Acta* 54 (2009) 4783-4788
- 26 S. Zhang, K. Xu, T.R. Jow. *Electrochim. Acta* 51, 1636-1640 (2006)
- 27 M. Kerlau, M. Marcinek, V. Srinivasan, R.Kostecki. *Electrochim. Acta* 53 (2007) 1385-1392
- 28 IEEE 1625. “Standard for Rechargeable Batteries for Mulit-Cell Mobile Computing Devices” IEEE Power & Energy Society 3 Park Avenue New York, Ny 10016 USA (2008)
- 29 P. Ramadass. *J. Power Sources* 112 (2002) 606-613
- 30 R. Kostecki. *J. Electrochem. Soc.* 153 (2006) A669-A672
- 31 C. Huang. *Electrochim Acta* 54, (2009) 4783-4788 (2009)
- 32 D. Aurbach, *Electrochim Acta* 00, 1-13 (2002)
- 33 J. Swart, D. Slee. (2008) doi: 10.1109/PSES.2008.4667528
- 34 C. Mikolajczak, T. Hayes, M. Megerle, M. Wu. (2007)

doi:10.1109/PORTABLE.2007.53

- 35 J. Remmlinger, (2010), doi: 10.1016/j.jpowsour.2010.08.035
- 36 R.B. Wright . J. Power Sources 119–121 (2003) 865-869
- 37 S. Zhao Electrochem. Commun. 12, 242-245 (2010)
- 38 R. Ramasamy, R. White, B. Popov. J. Power Sources 141, 298-306 (2005)
- 39 M. Itagaki, N. Kobari, S. Yotsuda. K. Watanabe, S. Kinoshita, M. Ue. J. Power Sources 135, 255-261 (2004)
- 40 David Linden, Handbook of batteries & Fuel Cells (McGraw-Hill, Inc 1984), pp. 16-25
- 41 B.Liaw, G. Nagasubramanian, R. Jungst, D. Doughty. Solid State Ionics 175, 835-839 (2004)
- 42 M. Mirzaeian, P.J. Hall. J. Power Sources 195, 6817-6824 (2010)
- 43 G. Plett. J. Power Sources 134, 277-292 (2004)
- 44 D. Zhang. J. Power Sources 91, 122-129 (2001)
- 45 L. Chen, Electrochim. Acta 51, 5548-5555 (2006)
- 46 D. Baert, A. Vervaet. (2001) doi:10.1049/cp:20010614
- 47 A. Delaille, M. Perrin, F. Huet. L. Hernout. J. Power Sources 158, 1019-1028 (2006)
- 48 Y. Itou, Y. Ukyo. J. Power Sources 146, 39-44 (2005)
- 49 C. Wu, Y. Bai, F. Wu. J. Power Sources 189, 89-94 (2009)
- 50 Peled, Golodnitsky, Ulus, V.Yufit. Electrochim. Acta 50, 391-395 (2004)
- 51 S.Chi, J. Son, Y.Yoon, J. Kim. J. Power Sources 158, 1419-1424 (2006)
- 52 F. Orsini J. Power Sources 76, 19-29 (1998)
- 53 S. Jeong, M Inaba, Y. Iriyama, T. Abe, Z. Ogumi. Electrochim. Acta 47, 1975-1982 (2002)
- 54 Weihe Kong, Hong Li, Xuejie Huang, Liquan Chen. J. Power Sources 142, 285-291 (2005)
- 55 Q. Wang, J. Sun, X. Yao, C. Chen. Thermochim. Acta 437, 12-16 (2005)

- 56 Material Safety Data Sheet, Li-Ion batteries. Ansmann 2006
- 57 R.E. Gosselin, R.P. Smith, H.C. Hodgge, Clinical Toxicology of Commercial Products (Williams and Wilkins, Baltimore, 1984)
- 58 M. Archuleta. J. Power Sources 54, 138-142 (1995)
- 59 National Library of Medicine Toxicology Data Network; *Hazardous Substance Data Bank (HSDB)*, Toxnet, 1994.
- 60 Material Safety Data Sheet: HF-0013. Honeywell 2002
- 61 S.Zhang. J. Power Sources 162, 1379-1394 (2006)
- 62 H.J. Santer. J. Power Sources 119-121, 368-371(2003)
- 63 Material Safety Data Sheet “Acrylonitrile” Science Lab.com, Inc
- 64 H.S. Lee, X.Q. Yang, C.L. Xiang, J. McBreen, L.S. Choi, J. Electrochem. Soc. 145, 2813 (1998)
- 65 H. Arai, S. Okada, Y. Sakurai, J.Yamaki. Solid State Ionics 95, 275-282 (1997)
- 66 H. Arai, S. Okada, Y. Sakurai, J.I. Yamaki, Solid State Ionics 109, 295 (1998).
- 67 T. Ohzuku, A. Ueda, M. Kouguchi, J. Electrochem. Soc. 142, 4033 (1995)
- 68 C.W. Kwon, S.E. Cheon, J.M. Song, H.T. Kim, K.B. Kim, C.B. Shin, S.W. Kim. J. Power Sources 93, 145-150 (2001)
- 69 Ziyang Zhang, Kanghua Chen, Erfu Ni. J. Electroanal. Chem. 645, 81-86 (2010)
- 70 K. Ozawa, Solid State Ionics 69, 212 (1994)
- 71 P.G. Balakrishnan, R.Ramesh, T. Prem Kumar. J. Power Sources 155, 401-414 (2006)
- 72 S.W. Eom. J. Power Sources 174, 954-958 (2007)
- 73 HP Recalls Notebook Computer Batteries Due to Fire Hazard (U.S. Consumer Product Safety Commission 2009)
<http://www.cpsc.gov/CPSCPUB/PREREL/prhtml09/09221.html>. Accessed 12 January 2011

- 74 National Research Council Recommendations Concerning Chemical Hygiene in Laboratories. (1910.1450 App A. Occupational Safety and Health Standards) www.osha.gov. Accessed 12 January 2011
- 75 J.R. Dahn, U. von Sacken, H. Al-Janaby, M.W. Juzkow, *J. Electrochem. Soc.* 138, 2207 (1991)
- 76 A. Magistris, P. Mustarelli, E. Quartarone, C. Tomasi. *Solid State Ionics* 136-137, 1241-1247 (2000)
- 77 D. Aurbach, B. Markovsky, G. Salitra, E. Markevich, Y. Talyossef. *J. Power Sources* 165, 491-499 (2007)
- 78 M. Lain. *J. Power Sources* 97-98, 736-738 (2001)
- 79 R.A. Huggins. *J. Power Sources* 153, 365-370 (2006)
- 80 M Smart. B Ratnakumar. *Electrochem. Soc.* 802 1282 (2008)
- 81 A. Hightower, C.C. Ahn, B. Fultz. *Appl. Phys. Lett.* 77, 2
- 82 N. Choi, I. Profatilova, S. Kim, E. Song. *Thermochim. Acta* 480, 10-14 (2008)
- 83 UL Standard for Safety for Lithium Batteries, UL1642. Underwriters Laboratories Inc. Northbrook, IL 1995
- 84 Self-Discharge analysis of LiCoO₂ for lithium batteries Sun Hee Choi, Joosun Kim, Young Soo Yoon. *Journal of Power Sources* 138 (2004) 283-287
- 85 An investigation of intercalation-induced stresses generated during lithium transport through LiCoO₂ film electrode using a laser beam deflection method. Su-II Pyun, Joo-Young Go, Tae-Seok Jang. *Electrochimica Acta* 49 (2004) 4477-4486
- 86 Kinetics of lithium intercalation into carbon anodes: in situ impedance investigation of thickness and potential dependence. Evgenij Barsoukov, Jong Hyun Kim, Jong Hun Kim, Chul Oh Yoon, Hosull Lee. *Solid State Ionics* 116 (1999) 249-261

- 87 Screening Li-ion Batteries for internal shorts. Eric Darcy, Journal of Power Sources
174 (2007) 575-578
- 88 Andrew T. Stamps, Charles E. Holland, Ralph E. White, Edward P. Gatzke. "Analysis
of capacity fade in a lithium ion battery" Journal of Power Sources 150 (2005) 229-
239